Author's Responses

First of all, we would like to thank the reviewers for their efforts. The comments and questions have been very helpful for improving the manuscript. We provided a point-by-point responses to the reviewers' comments, additional changes and corrections, and the marked up manuscript version showing the changes made in red strikethrough and underlines.

Response to the Reviewer #1

Please find below the reviewer comments in black, followed by the author's response in blue.

General comment:
The article presented by Sakai et al. is within the topics of AMT. It is clear in its approach and presents a very detailed validation of a new H2O Raman lidar. In addition, the opportunities offered by the water vapor lidars are relevant considering the increase of the extreme raining events. It deserves to be published. I have some minor corrections and remarks listed in the following.

Thank you for reading our manuscript and giving insightful comments and suggestions. We have read your comments carefully and revised the manuscript in accordance with the suggestions. Please find our point-to-point answers below.

1) Abstract L15: Changed their by the Introduction The requirement for data assimilation is more on the absolute value of the root-mean-square-error, less than 0.4 g/kg in the planetary boundary layer (Weckwerth et al). Biases are more problematic for data assimilation process and may induce large discrepancies.

In accordance with the reviewer's suggestion, we have provided the absolute values of the RMSD (0.98 g/kg) as well as the relative error in the abstract, which is larger than the required value of 0.4 g/kg reported by Weckwerth et al. (1999). However, in a recent review by Wulfmeyer et al. (2015) reported that the noise error lower than 10% and bias error smaller 5% are required for the data assimilation. These values can be translated into <1 g/kg and < 0.5 g/kg for 10 g/kg that is typical value in the lower troposphere. Thus, we have provided these percentage values as follows.

P1, L14-16: "The comparison results showed that MRL-derived w agreed within 10% (root-mean-square difference of 0.98 g/kg) with values obtained by radiosonde at altitude ranges".
P2, L1-2: "Wulfmeyer et al. (2015) discussed the requirements of accuracy of the lower tropospheric water vapor measurement for data assimilation and reported that it should be smaller than 10% in noise error and < 5% in bias error."
P16, L26-28: "Our comparison of the MRL-derived w values with those obtained with collocated radiosondes showed that they agreed within 10% and RMSD with 0.98 g/kg between altitudes of 0.14 and 5–6 km at night and between altitudes of 0.14 and 1.5 km in the daytime."

2) Section 2.4: The investigation about the variation of K is a very interesting study. From our experience, it may be due to temperature instabilities in the trailer, although in our case we could not pinpoint whether it was due to PMT gain or filter CWL variations. Maybe the temperature of the air conditioning was set differently during the summer and the fall? The high voltages of the photomultipliers seem to be fixed; some authors vary the PMT gains to

adjust for the signal/sky background noise ratio during daytime and nighttime. This means the PMT gain has been optimized for daytime limitations, and that the lidar could be more effective at night. Could you comment? Why was it necessary to adjust the focus? Because of the displacement of the trailer? Is your collimating lens an achromat? If not, it could explain the change of K with the change of focus.

We set the temperature of the air conditioner 23°C during the summer and autumn. The variation of the temperature in the trailer was at most ± 5 K (21-28°C). According to the manufacturers, the temperature variation of the sensitivity of PMT is <0.4%/K (Hamamatsu Photonics, 2017) and that of the filter CWL is < 0.0035 nm/K (FUJITOK, Japan, personal communication), which corresponds to <6% variation of the effective Raman backscattering cross section ratio (N_2 / H_2O) for ± 5 K variation (Fig. A1). Accordingly, we have added comments on these variations to Section 2.4 as follows.

P6, L13-16: "During the experimental period, the variation of temperature in the trailer was at most ± 5 K, which corresponds to <6% variation of the effective Raman backscattering cross section ratio and thus *K*, assuming that the temperature variation of the sensitivity of PMT is <0.4%/K (Hamamatsu Photonics, 2017) and that of the filter CWL is < 0.0035 nm/K (FUJITOK, Japan, personal communication)."

As the reviewer has suggested, changing the high voltages of the PMTs during daytime and nighttime is effective to optimize the PMT gain. During the experiment in 2016, we did not change the high voltages (i.e. –1300 V) so that the measurement performance was limited. In particular, the sensitivity of PMT decreased around midday in Summer when the solar zenith angle is high. To improve the performance, we upgraded the lidar control program to automatically change the high voltages during day and night in 2018.

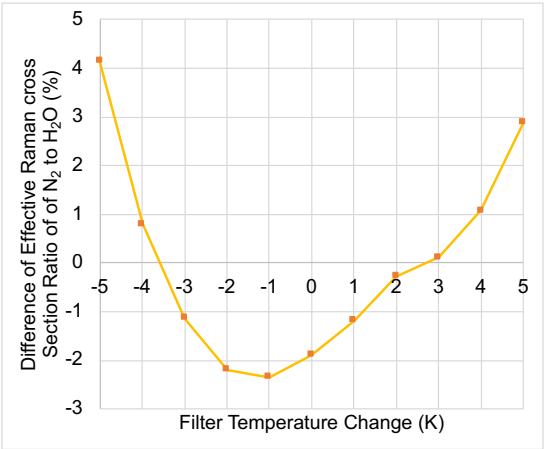

Figure A1. Calculated differential effective Raman backscattering cross section ratio of N_2 to H_2O channels as a function of interference filters used in this study.

3) Section 2.5: To improve the calibration process, especially for the overlap correction function in the lower layers, tethered balloon or kite can be used as in Totems and Chazette (2016). We are then certain of the location of the reference measurements, and we can renew it at will. The accuracy on w is then better. Totems, J. and Chazette, P.: Calibration of a water vapour Raman lidar with a kite-based humidity sensor, Atmos. Meas. Tech., 9, 1083-1094, doi:10.5194/amt-9-1083-2016, 2016. Could you comment on whether this correction of the overlap factor needs to be re-evaluated at the same time as K when the telescope is re-

aligned/re-focused? Rather than PMT inhomogeneity, the incidence on the interference filters may have been modified by the change of focus, which is known to have a large impact.

The use of kite for the lidar calibration and determination of the overlap function is a promising method because it can measure the air close to the lidar. We think that unmanned aerial vehicle can be also used for that purpose. One important issue for use of them is that we need to get permission of the Minister of Land, Infrastructure and Transport if we fly it over a height of 150 m in a densely populated area or near airport in Japan. In accordance with the suggestion, we have added the comment with the reference paper (Totems and Chazette, 2016) to Section 2.5 as follows.

P7, L11-13: "The variation should be reduced if using the data measured above the lidar by using a kite (Totems and Chazette, 2016) or unmanned aerial vehicles."

We agree that the correction of the overlap needs to be re-evaluated when the telescope is re-aligned/refocused. Thank you for the information that change of the telescope's focus has large impact on K by modifying the incidence on the interference filters that.

4) In Figure 5, there is a great variability of the observed overlap correction, what can explain this? Lidar noise? Radiosounding error? It may be necessary to distinguish different cases because it is an important point for the robustness of the measurement in the lower tropospheric layers. Can you evaluate or at least comment on the resulting uncertainty on w below 1 km altitude?

We have checked the individual profile of the comparison of w between the lidar and radiosounding (Fig. S1) . It is difficult for us to distinguish the reasons for the variability. The possible reasons are 1) the difference of the measurement period and the temporal resolution (i.e. 20 minutes average for the lidar and approximately 1 second for the radiosonding), 2) the difference of the vertical resolution (i.e. 75 m for the lidar and 20–300 m (it depends on the significant pressure level interval) for the radiosounding data), and 3) lidar noise. The uncertainty of the correction was estimated to be 8% from the standard deviation of the difference between the lidar and radiosounding as follows.

P7, L8-11: 'The uncertainty of the correction was estimated to be 8% from the standard deviation of the profiles. The possible reasons for the variation among the profiles are difference of the measurement period and temporal resolution (i.e. 10 minutes average for the lidar and approximately 1 second for the radiosonde), difference of the vertical resolution (i.e. 75 m for the lidar and 20–300 m that depends on the significant pressure level interval for the radiosonde, and lidar noise."

5) Section 3.1.1: Radiosounding errors should also be shown in Figure 6.

We have added the error bars of the radiosonding in Fig. 6.

6) L24-27: The decrease of the water vapor concentration could be seen on the in-situ measurements of weather stations. Perhaps the temporal evolution of one of these measurements should be added. Why would the laser energy have decreased? Is it because of cold, flash lamps and/or damage on optics? The differences with the modeling can be related to local effects and thus to the representativity of the measurement site at the mesoscale.

They can also be due to a problem in the assimilation process if it does not integrate well the error matrices.

Because the decrease of the water vapor concentration can be seen in Fig. 9, we would like to retain the figure without showing the temporal evolution of *w* at the surface. Instead, we have added the comment to the Section 3.1.1 that the monthly mean *w* values decreased from 17 to 4 g/kg at 1000 hPa and from 8 to 1 g/kg at 700 hPa between August and December in 2016 as follows.

P8, L30-32: "As for the water vapor concentration, the monthly mean w values decreased from 17 to 4 g/kg at 1000 hPa and from 8 to 1 g/kg at 700 hPa between August and December
in 2016."

The primary reason for the decrease in the laser power was the aging of the flash lamp because the emission power decreases as increasing shot number (the lifetime is 20 million shots, or about 3 weeks for the continuous operation). In fact, the laser power increased from 110 mJ/pulse to 220 mJ/pulse after replacing the flash lamp and adjusting the angles of second and third harmonic crystals after the experiment on 8 December 2016. We have added the comment to Section 3.1.1 as follows.

P8, L29-30: "As for the laser power, it increased from 110 mJ/pulse to 220 mJ/pulse after replacing the flash lamp and adjusting the angles of second and third harmonic crystals on 8 December 2017."

We agree with you that the differences with the modeling can be related to local effects and thus to the representativeness of the measurement site at the mesoscale. We have added the comment to Section 3.3.2 as follows.

P14, L23-25: "The differences with the LA data can be related to local effects and thus to the representativeness of the measurement site at the mesoscale. They can also be due to a problem in the assimilation process if it does not integrate well the error matrices."

7) Section 3.1.2, L11: Typing error on "difference-wsonde"?

We have deleted the word because it is unnecessary.

8) Section 3.1.3: This section should be merged with section 3.1.1.

We have merged Section 3.1.3 with Section 3.1.1 in accordance with the reviewer's suggestion. To be consistent with this change, we have changed the order of subsections in Section 3.3.

9) Section 3.2, L11: A ground level in-situ measurement could have helped.

Following the reviewer's suggestion, we used the ground level in-situ measurement of *w* to compute PWV from the lidar data instead of interpolating the lidar-derived w at 0.14 km to the ground level. By this change, the lidar-derived PWV values has slightly changed and thus result of the comparison between RL- and GNSS-derived values also changed as follows. The slope and intercept of the regression changed from 0.968 to 0.967 and from −0.229 mm

to −0.142 mm, respectively, and RMSD decreased from 2.88 mm to 2.84 mm. We have updated these values in Table 3. In addition, we have modified the explanation of the method of calculating PWV values as follows.

P12, L15-16: "Below 0.1 km, we interpolated the *w* data to the ground level in-situ measurement."

10) Section 3.3.1: It is not so clear whether assimilation is only about radiosounding. Are there no other types of data assimilated, such as spaceborne data? It would be better to show the scatter plot of the radiosounding/LA also.

The LA assimilates the multiple sources, including surface measurements, radiosounding, satellites, and GNSS-derived PWV data, as has been described in Section 3 (P7, L27-28). Because the main purpose of this paper is the validation of the RL system, we would like to show the scatter plot of the radiosounding and LA only in Fig. A2 in this response but not in the original manuscript. We can see in Fig. 2A that there was a negative bias in the LA data.

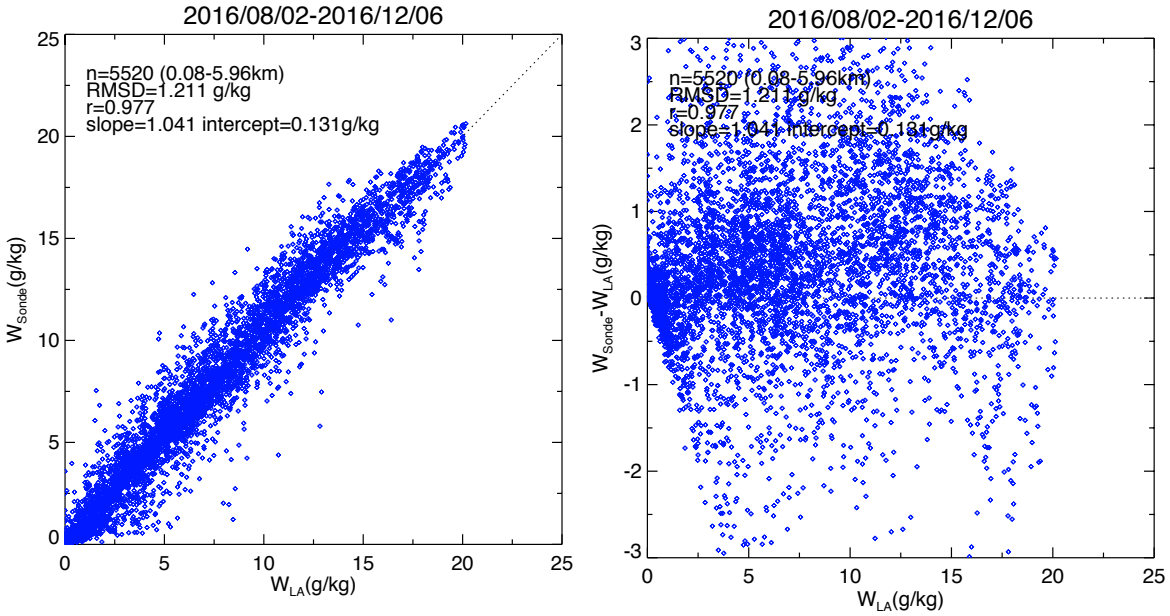

Fig. A2. (Left panel) Scatter plot of *w* obtained with the LA (w_{LA}) versus *w* obtained with radiosondes (w_{Sonde}) from 2 August to 6 December 2016. (Right panel) Scatter plot of the difference ($w_{LA} - w_{Sonde}$) as a function of w_{LA}.

11) Section 4: Change numbering.
Collected.

References:

Hamamatsu Photonics K. K. (2017), Photomultiplier tubes, basics and applications, 3rd Ed., Figures 8-11 and 13-1 (available from https://www.hamamatsu.com/resources/pdf/etd/PMT_handbook_v3aE.pdf).

Weckwerth, T. M., V. Wulfmeyer, R. M. Wakimoto, R. M. Hardesty, J. W. Wilson, and R. M. Banta (1999), NCAR-NOAA lower tropospheric water vapor workshop, *Bull. Am. Meteorol. Soc.*, 80, 2339–2357.

Wulfmeyer, V., R. M. Hardesty, D. D. Turner, A. Behrendt, M. P. Cadeddu, P. Di Girolamo, P. Schlüssel, J. Van Baelen, and F. Zus (2015), A review of the remote sensing of lower

tropospheric thermodynamic profiles and its indispensable role for the understanding and the simulation of water and energy cycles, *Rev. Geophys.*, 53, doi:10.1002/2014RG000476.

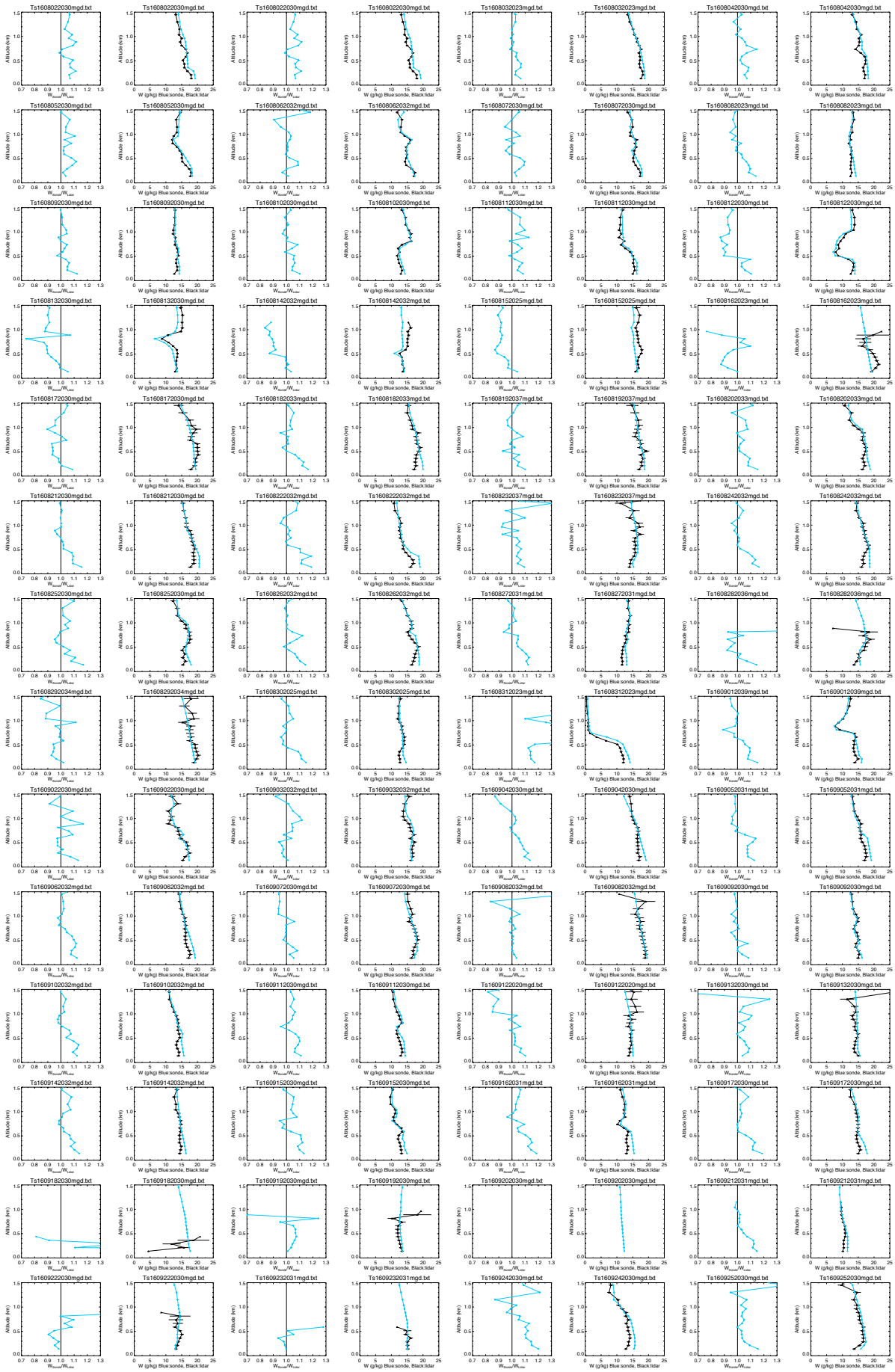

Figure S1. Vertical distribution of the ratio of *w* obtained by radiosonde (light blue) to *w* obtained with the RL system without beam overlap correction (black) from 2 August to 6 December 2016.

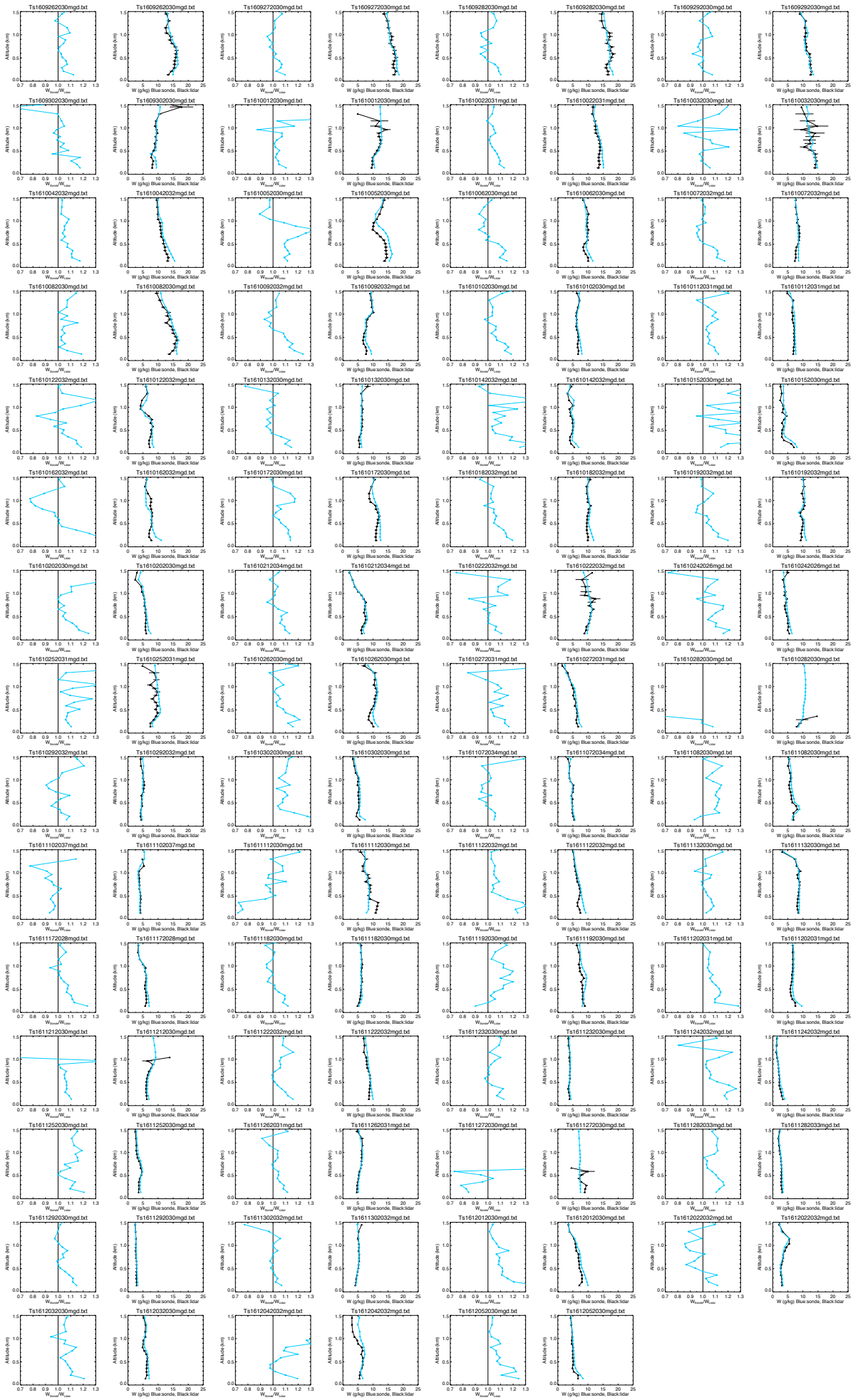

Figure S1. (Contd.)

Response to the Reviewer #2:

Please find below the reviewer comments in black, followed by author's response in blue.

1) The manuscript by Sakai et al. mainly describes the designing and the performances of an automatic Raman lidar system designed for the measurement of water vapor mixing ratio profile during daytime and nighttime conditions. According to the authors, the final goal of the work is to show the positive impact that water vapour Raman lidar measurements may potentially have if assimilated in a heavy-rain forecasting system.
The manuscript is sufficiently well written and outlines in detail the experimental setup of the Raman lidar. The stability of the Raman lidar calibration is assessed over the test period of the instruments, while the correction for the system incomplete overlap is calculated using radiosounding data from a nearby station. Intercomparison statistics versus radiosoundings and GNSS measurements for both the profile and the integrated water vapor content are used to validate the Raman lidar measurements.
Regardless of my specific concerns about the conclusions presented by the authors to support the validation of the Raman lidar measurements, more in general, I think that this manuscript does not demonstrate what the title would like to claim, i.e. the positive impact of the Raman lidar measurements on an heavy rain forecasting model.

Thank you for the critical comments on our manuscript. We agree with your claim that the manuscript does not show the final goal that is to show the positive impact of the lidar measurements on a heavy rain forecasting model. However, we would like to say that this is the first step of our study aiming to the goal, that is to say, to describe the experimental setup of the low-cost mobile Raman lidar and the validation of measurement by comparisons with other humidity sensors and model. To clarify the purpose of this manuscript and avoid potential misleading, we would like to change the title to "Mobile water vapor Raman lidar for heavy rain forecasting: instrument description and comparison with radiosonde, GNSS, and high-resolution objective analysis".

The study on the impact of using lidar data on the heavy rain forecast with a nonhydrostatic mesoscale model has already been published in English (Yoshida et al. 2018a) that showed a positive impact on the humidity fields that were analyzed and forecasted with the model. More detailed description of the assimilation experiments will be submitted to a peer-reviewed journal soon (Yoshida et al. 2018b). Accordingly, we have changed the former reference in Japanese to these papers in the revised manuscript. Although the current manuscript does not show the positive impact of the Raman lidar measurement on the heavy rain forecasting model, we believe that it meets the main subject area of AMT that comprise the development, intercomparison, and validation of the measurement instruments.

2) Focusing on the section where the comparison with high resolution local analysis data is reported, the authors' expectation is to demonstrate, from the Observation minus-Background (O-B) comparison on a limited time period (less than 5 months), that the Raman lidar can improve the rain forecasting system because it is able to reveal an evident bias in the analysis model output.
－This is indeed a demonstration of the well known value of Raman lidar measurement to assess the performance of the model analysis output.

We agree with you that the Raman lidar can reveal the bias of the model analysis output. We think that this finding (i.e. positive bias in the local analysis model output from the lidar data) is one important outcome of the study. This has been noticed in Section 3.1.1.

3) To demonstrate the impact of lidar observations on any forecasting system a data assimilation experiment or alternatively an Observing System Simulation Experiments (OSSE) must be carried out. Various examples are available in literature of lidar data assimilation experiments (e.g. Wulfmeyer et al., 2006, https://journals.ametsoc.org/doi/10.1175/MWR3070.1). The authors state that they are currently studying the impact of using lidar data with a nonhydrostatic mesoscale model for simulating heavy rainfall in the Kanto area in Summer 2016, citing a paper in Japanese: to my opinion the outcome of these experiment must be embedded in the manuscript by Sakai et al. because it could be the only possibility to add more substance to the manuscript and create a real scientific interest in the readers.

As stated earlier, we would like to publish separately the result of the data assimilation experiment from this manuscript because a substantial amount of description is needed to fully describe the result. To convince the readers that the lidar data has a positive impact on the heavy rainfall forecasting, we added a brief summary of the result of the assimilation experiments by Yoshida et al. (2018a, b) to Section 3.4 as follows.

P16, L14-17: "A first assimilation experiment of the MRL-derived vertical profiles of w into the JMA-NHM using the three-dimensional LETKF for the heavy rainfall forecasting has been reported by Yoshida et al. (2018a), who showed a positive impact on the analyzed and forecast humidity fields on the Kanto Plain on 17 August 2016. More detailed description of the assimilation experiment will follow soon (Yoshida et al. 2018b)."

4) In addition, the lidar described in the manuscript does not add new knowledge about innovative, more advanced technological solutions than the other home-made and commercial Raman lidars operating around the world. Besides, also about the intercomparison of Raman lidar measurements with radiosoundings, GNSS, MWR and FTIR, many other papers are available in literature using more robust approaches (Bhawar et al., 2011, https://rmets.onlinelibrary.wiley.com/doi/pdf/10.1002/qj.697; Beherendt et al., 2007, https://journals.ametsoc.org/doi/full/10.1175/JTECH1924.1).

Thank you for introducing the papers on the validation of Raman lidars. By reading those paper, we found that there are more robust approaches of the intercomparison than ours. However, we think that our approach is still useful for the validation because the distances of the measurement instruments were much smaller (less than 100 m) than them.

In response to your claim that the manuscript does not add new knowledge about innovative or more advanced technological solutions than the existing Raman lidar, we would like to point out that one advanced technological solution of the MRL is that it can be easily deployed to remote site and start the measurement in a few hours after the deployment. That is very beneficial for investigating measurement locations that are effective for the heavy rain forecasting. To our knowledge, such a small mobile Raman lidar has only been reported by Chazette et al. (2015) and few intercomparison paper has been available. To emphasize the new aspects of our developments and studies, we have added these comments to the abstract and the Introduction section of the revised manuscript as follows.

P1, L11-13: "The MRL was installed in a small trailer for easy deployment to the upwind side of potential rainfall areas and can start measurement in a few hours to monitor the inflow of moist air before rainfall events."

P1, L29-30: “The MRL can be easily deployed at a site upwind of a potential heavy 30 rainfall area and start measurement in a few hours to monitor the vertical water vapor distribution before a rainfall event.”
P2, L10: “To our knowledge, there are few reports on the validation for such a compact mobile system.”

5) The authors themselves, when trying to assess of the Raman lidar system performance which should be able to provide continuous profile of the water vapor mixing ratio, they do clearly show that during daytime the lidar has very limited performance, providing measurements with an uncertainty lower than 30% up to about 1.0-1.5 km above the ground level, which is also the region where the overlap correction is applied. These performances are even lower than a few of commercial Raman lidars and for sure does not allow to achieve the desired impact on a data assimilation system.
However, as I said before the impact must be concretely demonstrated and the considerations provided in the manuscript are not sufficient to this purpose.
I must also note that the authors honestly acknowledge that the maximum measurement altitude achievable with the Raman lidar system is limited during the daytime and that, though in theory this does not prevent the data assimilation (though I am concerned about the total uncertainty budget in this region), there are the limited information provided by the lidar in the boundary layer and obviously above.

Even though the maximum measurement altitude is limited to 1.0-1.5 km in daytime, it is still useful for the heavy rain forecast because the height of the inflow of moist air that can cause heavy rainfall downwind is mostly around 0.5 km in Japan (Kato, 2018). Moreover, Yoshida et al. (2018a) has shown a positive impact of the MRL data on the analyzed and forecast humidity fields as mentioned before. We also note that we intendedly limited the performance of the lidar (but still meets our requirement) to reduce the total material cost (< 250K US dollars) because it makes easier to distribute the MRL around the forecasting areas to increase the opportunity of detecting inflow. We have added this comment to the Introduction section of the revised manuscript as follows.

P2, L3-5: “Besides the requirement of measurement accuracy, reducing the cost of the lidar is important because it makes easier to distribute them around the forecasting area to increase the opportunity of detecting the inflow. We developed our mobile MRL system to meet these requirements as much as possible within the total material cost of ~250K USD.”

As for the overlap correction, we estimate that the total uncertainty is at most 23% (10% for the calibration coefficient, 8% for the overlap correction, and <5% for the signal noise) where the overlap correction is applied. We have provided the estimated values of the uncertainty of the overlap correction in Section 2.5 as follows.

P7, L8: “The uncertainty of the correction was estimated to be 8% from the standard deviation of the profiles.”

6) This pushes the authors to state that the development of a diode laser-based differential absorption lidar (ongoing) will allow to improve the range and the quality of the measurement for their rain forecasting system. This statement sounds like a "certification" of the insufficient performance of the Raman lidar for the proposed objective. Therefore, I’d propose the manuscript rejection, but I hope to see the authors submitting soon a new

manuscript showing concrete results related to the impact of DIAL measurements or, at least, of the current night time Raman lidar measurements on a rain forecasting system.

Thank you for encouraging us to further study to improve heavy rain forecasting system. Improving the forecast accuracy and lead time of heavy rain is an urgent issue in Japan. In fact, heavy rain caused floods and landslides that killed over a hundred of people in the southwest Japan in June 2016, July 2017, and July 2018. So we decided to develop the MRL at first before completion of the development of the diode-laser-based DIAL even though the measurement performance was limited. We think that this manuscript is an important step of our study.

References:

Chazette, P., Marnas, F., and Totems, J.: The mobile water vapor aerosol Raman LIdar and its implication in the framework of the HyMeX and ChArMEx programs: application to a dust transport process, Atmos. Meas. Tech., 7, 1629-1647, https://doi.org/10.5194/amt-7-1629-2014, 2014.

Kato, T., Representative height of the low-level water vapor field for examining the initiation of moist convection leading to heavy rainfall in East Asia. J. Meteor. Soc. Japan, 96, 68-83, https://doi.org/10.2151/jmsj.2018-008, 2018.

Yoshida, S., T. Sakai, T. Nagai, S. Yokota, H. Seko, Y. Shoji: Feasibility study of data assimilation using a mobile water vapor Raman lidar, Proceedings of the 19th conference on coherent laser radar technology and applications, p251-255, https://clrccires.colorado.edu/data/paper/P21.pdf, 2018.

Yoshida, S., T. Sakai, T. Nagai, S. Yokota, H. Seko, and Y. Shoji: Data assimilation of water vapor mixing ratio observed by a lidar to forecast heavy precipitation, J. Meteor. Soc. Japan, (to be submitted), 2018b.

Additional changes and corrections

- We have changed the abbreviation of the mobile Raman lidar from mobile RL to MRL for simplicity.

- We have added the abbreviations of the nonhydrostatic mesoscale model (NHM) and the local ensemble transform Kalman filter (LETKF) because they were used in Section 3.4.

- Figure 1 has been modified because the position of the PMTs of the Raman nitrogen and elastic channels was reversed.

- We have corrected the manufacture's name and type of the shortcut filters (Isuzu Glass ITY385, Japan) and added them of the shortpass filters (SHPF-50S-440, SIGMAKOKI, Japan) in Section 2.

- We have changed the title of Section 3.4 from "Summary of the validation results" to "Summary of the validation results and outlook" to clarify the content of the section.

- We have updated the reference paper by Kato et al. (2014) to Kato (2018) in English.

Mobile water vapor Raman lidar for heavy rain forecasting: ~~system~~ instrument description and validation by comparison with radiosonde, GNSS, and high-resolution objective analysis

Tetsu Sakai[1], Tomohiro Nagai[1], Toshiharu Izumi[2], Satoru Yoshida[1], Yoshinori Shoji[1]

[1]Meteorological Satellite and Observation System Research Department, Meteorological Research Institute, Tsukuba, 305-0052 Ibaraki, Japan
[2]Observation Department, Japan Meteorological Agency, 1-3-4 Otemachi, Chiyoda-ku, 100-8122 Tokyo, Japan

Correspondence to: Tetsu Sakai (tetsu@mri-jma.go.jp)

Abstract. To improve the lead time and accuracy of predictions of localized heavy rainfall, which can cause extensive damage in urban areas in Japan, we developed a mobile Raman lidar (MRL) system for measuring the vertical distribution of the water vapor mixing ratio (w) in the lower troposphere. The ~~RL~~ MRL was installed in a small trailer for easy deployment to the upwind side of potential rainfall areas and can start measurement in a few hours to monitor the inflow of moist air before rainfall events. We describe the ~~lidar~~ MRL system and present validation results obtained by comparing the ~~RL~~ MRL-measured data with collocated radiosonde, Global Navigation Satellite System (GNSS), and high-resolution objective analysis data. The comparison results showed that ~~RL~~ MRL-derived w agreed within 10% (root-mean-square difference of 0.98 g/kg) with values obtained by radiosonde at altitude ranges between 0.14 and 1.5 km in the daytime and between 0.14 and 5–6 km at night in the absence of low clouds; the vertical resolution of the ~~RL~~ MRL measurements was 75−150 m, their temporal resolution was less than 20 min, and the measurement uncertainty was less than 30%. ~~RL~~ MRL-derived precipitable water vapor values were similar to or slightly lower than those obtained by GNSS at night, when the maximum height of ~~RL~~ MRL measurements exceeded 5 km. The ~~RL~~ MRL-derived w values were at most 1 g/kg (25%) larger than local analysis data. Four months of continuous operation of the ~~RL~~ MRL system demonstrated its utility for monitoring water vapor distributions for heavy rain forecasting.

1 Introduction

In recent years, the occurrence frequency of localized heavy rainfall capable of causing extensive damage has been increasing in urban areas of Japan (Japan Meteorological Agency (JMA), 2016). For early prediction of heavy rainfall, a numerical weather prediction (NWP) model is employed along with conventional meteorological observation data. However, the lead time (period of time between the issuance of a forecast and the occurrence of the rainfall) and accuracy of the prediction are limited, in part, because of the coarse temporal and spatial resolutions of water vapor distribution observations. To improve those observations, we developed a low-cost mobile Raman lidar (MRL) system that can continuously measure the vertical distribution of water vapor in the lower troposphere. The ~~RL~~ MRL can be easily deployed at a site upwind of a potential heavy rainfall area and start measurement in a few hours to monitor the vertical water vapor distribution before a rainfall event. The observed data can then be assimilated into a nonhydrostatic mesoscale model (NHM) (Saito et al., 2007) by the local ensemble transform Kalman filter (LETKF) method (Kunii, 2014) to improve the initial condition of the water vapor field and consequently the rainfall forecast. We discussed with scientists involved in model development and implementation the required temporal and spatial resolution and accuracy of the measured data for heavy rain forecasting (Table 1). For example, Kato (~~2014~~2018) has reported that the equivalent potential temperature at a height of 500 m, which is a function of the water vapor concentration at that height, is an important parameter for forecasting heavy rainfall in the Japanese area because the inflow of moist air, which can cause heavy rain, mainly occurs at around that altitude. Thus, the measurable altitude range must extend upward to at least that altitude. In addition, the temporal resolution of the data should be better than 30 min,

because the assimilation window can be less than 30 min long. In addition, for data assimilation, the measurement uncertainty (observation error) must be specified. Wulfmeyer et al. (2015) discussed the requirements of accuracy of the lower tropospheric water vapor measurement for data assimilation and reported that it should be smaller than 10% in noise error and < 5% in bias error~~Wulfmeyer et al. (2015) discusses in more detail the requirements of measurements used for data assimilation~~. Besides the requirement of measurement accuracy, reducing the cost of the lidar is important because it makes easier to distribute them around the forecasting area to increase the opportunity of detecting the inflow. We developed our mobile ~~RL~~ MRL system to meet these requirements as much as possible within the total material cost of ~250K USD. The Raman lidar~~RL~~ technique is a well-established technique for measuring the water vapor distribution in the troposphere (e.g. Melfi et al., 1969, Whiteman et al., 1992), and ~~RL~~ the systems have been in operation for decades at stations around the world (Turner et al., 2016; Dinoev et al., 2013; Reichardt et al., 2012; Leblanc et al., 2012). Field-deployable systems have also been developed by several institutes (Whiteman et al., 2012; Chazette et al., 2014; Engelmann et al., 2016). Our ~~RL~~ MRL system is a compact mobile system that can be deployed on a standard vehicle and operated unattended for several months by remote control. To our knowledge, there are few reports on the validation for such a compact mobile system. As the first step of our goal aiming to develop the heavy rainfall forecasting system, ~~H~~here we describe our mobile lidar system and present validation results obtained by comparing the ~~RL~~ MRL-measured data with data obtained by other humidity sensors as well as objective analysis data. Section 2 of this paper describes the ~~RL~~ MRL instrumentation and the data analysis method. Section 3 presents the validation results obtained by comparing the ~~RL~~ MRL measurements with collocated radiosonde measurements, GNSS data, and high-resolution objective analysis data provided by the JMA. Section 4 is a summary.

Table 1. Lidar data requirements for localized heavy rain forecasting

System	Field deployable
Measured quantity	Water vapor mixing ratio (w)
Data description	
Altitude range	<0.2 km to >2 km
Time period	24-hour, continuous
Vertical resolution	<200 m
Temporal resolution	<30 min
Uncertainty	<10%

2 Instrumentation

2.1 Transmitter and receiver optics

The ~~RL~~ MRL system employs a Nd:YAG laser (Continuum Surelite EX) operating at 355 nm with pulse energy of 200 mJ and a repetition rate of 10 Hz. The beam diameter is expanded fivefold to a diameter of ~5 cm by a beam expander (CVI, USA), and the beam is emitted vertically into the atmosphere. The light backscattered by atmospheric gases and particles is collected by a custom-made Cassegrain telescope (primary mirror diameter of 0.35 m, focal length 3.1 m; Kyoei Co., Japan). The focal point of the telescope is within the tube to shorten the length of the receiving system. Light baffles placed inside the telescope tube prevent stray light from entering the detectors. The received light is separated into three spectral components, Raman water vapor (407.5 nm), nitrogen (386.7 nm), and elastic (355 nm) backscatter light, with dichroic beam splitters and interference filters (IFs) (Barr Materion, USA) ~~and~~ , shortcut filters (~~Kenko~~Isuzu Glass ITY385, Japan), and shortpass filters (SHPF-50S-440, SIGMAKOKI, Japan) and detected by photomultiplier tubes (PMTs) (R8619, Hamamatsu, Japan). The

interference filter angles of the Raman channels are tuned manually to maximize the transmission of the Raman backscatter signal. To avoid signal saturation of the PMTs, we inserted neutral density filters before the PMTs. The signals are acquired with a transient recorder (Licel TR-20-160) operating in analog (12-bit) and photon counting (20 MHz) modes. The data are stored on the hard disk of a personal computer (PC). The ~~RL~~ MRL can be operated remotely by issuing commands (e.g. turn high voltage of PMTs on/off, start/stop lasing, start/stop data acquisition, and transfer data) to the PC via wireless Internet communication (Table 2, Fig. 1).

Table 2. Specifications of the mobile Raman lidar

Transmitter:			
Laser	Nd:YAG		
Wavelength (nm)	355		
Pulse energy (mJ)	220 (maximum)		
Repetition frequency (Hz)	10		
Beam divergence (mrad)	0.125		
Receiver:			
Telescope type	Cassegrain		
Diameter of primary mirror (m)	0.35		
Field of view (mrad)	0.29		
Detectors	Photomultiplier tubes		
Data acquisition	Photon counting/analog		
Detection specifications:	Raman water vapor	Raman nitrogen	Elastic
Interference Filter			
Center wavelength (nm)	407.65	386.65	354.63
Bandwidth (nm)	0.25	0.34	0.6
Peak transmission (%)	74	45	43
Rejection at 355 nm	$<10^{-13}$	$<10^{-7}$	–

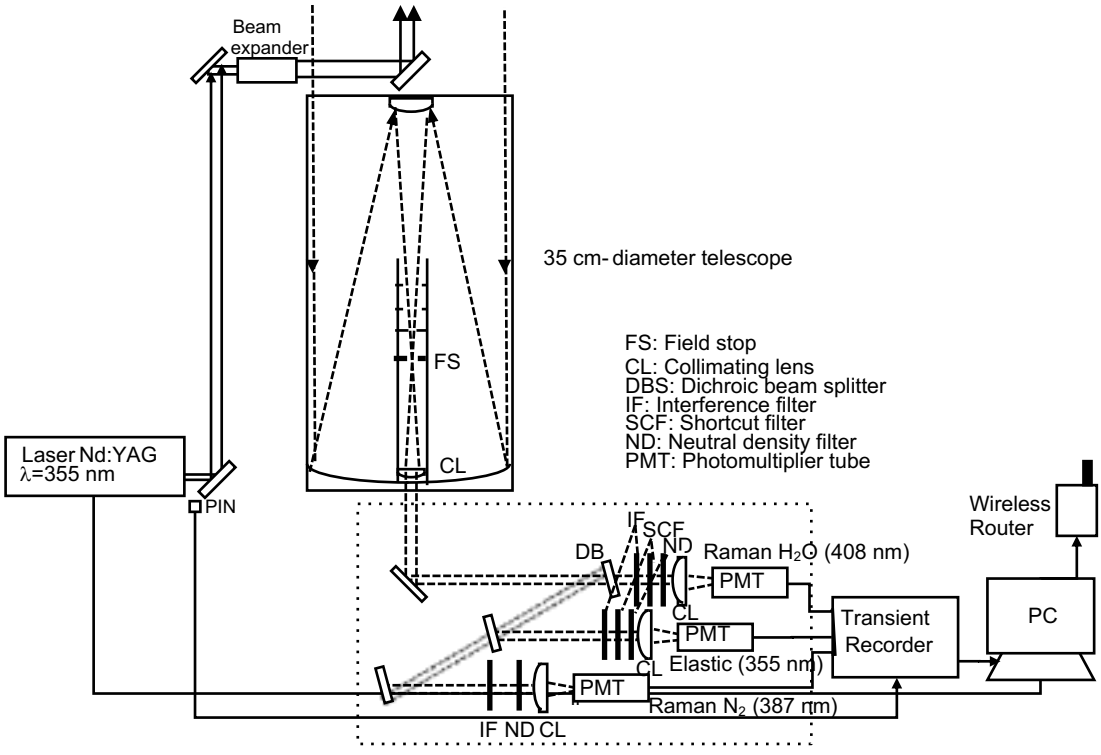

Figure 1. Schematic diagram of the mobile Raman lidar system.

2.2 Trailer

The ~~RL~~ MRL system is enclosed in a container with outside dimensions of 1.7 m by 4.2 m by 2.1 m high (Figs. 2 and 3). The total weight, including the lidar system and the trailer, is approximately 800 kg. The trailer can be towed behind any standard-sized vehicle; therefore, anyone who holds a basic-class driver's license can tow it in Japan. The temperature inside the trailer is maintained to 22–32 ºC by an air conditioner. A fused silica window (47 cm × 42 cm × 1 cm thick) with an antireflection coating installed at a tilt angle of 10° above the receiving telescope enables the ~~RL~~ MRL to be operated regardless of the weather. To prevent direct sunlight from entering the telescope, a chimney-type light baffle with a height of 2 m is mounted on top of the trailer. The system requires a single-phase, three-wire type 100/200V power supply with a maximum current of 10A (5–7 A during normal operation).

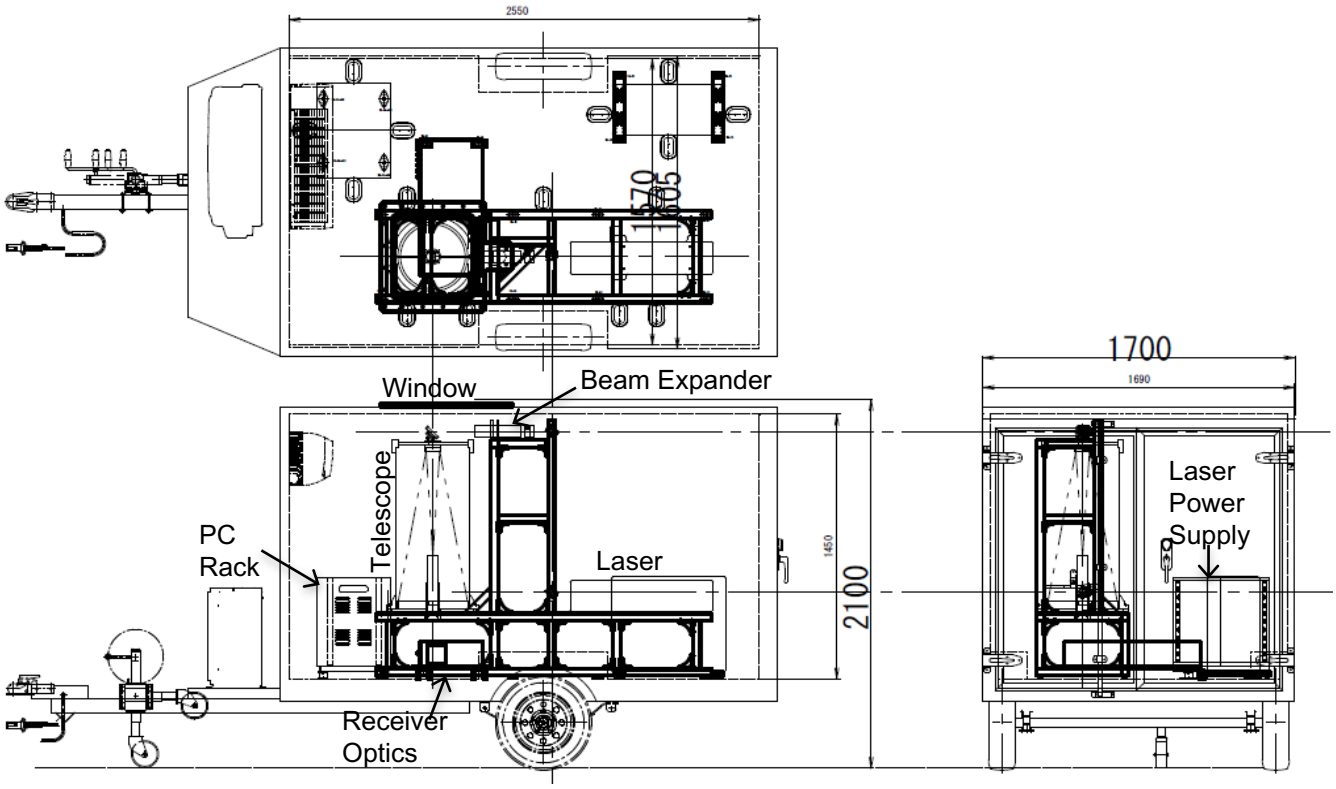

Figure 2. Layout of the mobile Raman lidar system in its trailer. Dimensions are in millimeters.

Figure 3. Photographs of the ~~mobile RL~~MRL trailer (left) and its interior (right).

2.3 Data analysis

The water vapor mixing ratio (w) is obtained from the observed Raman backscatter signal of water vapor and nitrogen as follows:

$$w(z) = K \frac{O_{H_2O}(z)}{O_{N_2}(z)} \frac{P_{H_2O}(z)}{P_{N_2}(z)} \Delta T(z_0, z),$$

with

$$\Delta T = \frac{e^{\int_{z_0}^{z} [\alpha_{H_2O}^{m}(z') + \alpha_{H_2O}^{p}(z')] dz'}}{e^{\int_{z_0}^{z} [\alpha_{N_2}^{m}(z') + \alpha_{N_2}^{p}(z')] dz'}},$$

(1)

where K is the calibration coefficient of the water vapor mixing ratio, $O_X(z)$ is the beam overlap function of the receiver's channel, and $P_X(z)$ is the noise-subtracted Raman backscatter signal of molecular species X (H_2O or N_2) at height z from the lidar at z_0, ΔT is the transmission ratio of the Ramen signals between the lidar at z_0 and z, and α_X^m and α_X^p are the molecular and particle extinction coefficients of X at the wavelength of the Raman scattering. The value of K was obtained by comparing the uncalibrated ~~RL~~ MRL-derived value of w (i.e. w computed assuming $K = 1$ in Eq. 1) with w obtained with a radiosonde launched 80 m northeast of the ~~RL~~ MRL at 20:30 LST by a weighted least squares method (Sakai et al., 2007) between altitudes of 1 and 5 km and taking the average over the measurement period. See Sect. 2.4 for the values of K obtained in this manner and their temporal variation. In this system, the ratio of the beam overlap functions ($\frac{O_{H_2O}(z)}{O_{N_2}(z)}$) is 1 above an altitude of 0.5 km, and below that altitude it deviates slightly from 1; these values were determined by comparing the ~~RL~~ MRL-derived value of w without overlap correction (i.e. w obtained by assuming $\frac{O_{H_2O}(z)}{O_{N_2}(z)} = 1$ in Eq. 1) with w obtained by radiosonde measurements (see Sect. 2.5). To determine ΔT, we calculated α_X^m using molecular extinction cross section (Bucholz, 1995) atmospheric density obtained from the radiosonde measurement made closest to the ~~RL~~ MRL measurement period; we did not take the differential aerosol extinction for the two Raman wavelengths into account because it is usually less than 5% below the altitude of 7 km (i.e. ΔT ranges from 1 to 0.95 from the lidar position to 7 km) under normal aerosol loading conditions (Whiteman et al., 1992). The temporal and vertical resolutions of the raw data were 1 min and 7.5 m, respectively. To reduce the statistical uncertainty of the derived w, we averaged the raw data over 20 min and reduced the vertical resolution to 75 m below 1 km

altitude and 150 m above that. The measurement uncertainty of w was estimated from the photon counts by assuming Poisson statistics (e.g. Whiteman, 2003) and the uncertainty of the calibration coefficient as follows:

$$\delta w(z) = \left[\left(\frac{\delta K}{K}\right)^2 + \left(\frac{\delta P_{H_2O}(z)}{P_{H_2O}(z)}\right)^2 + \left(\frac{\delta P_{N_2}(z)}{P_{N_2}(z)}\right)^2\right]^{\frac{1}{2}},$$

where

$$\delta P_X = \left(P_{X,signal} + 2P_{X,noise}\right)^{\frac{1}{2}}. \quad (2)$$

The signal ($P_{X,\,signal}$) was obtained from the total backscatter signal by subtracting the background noise ($P_{X,\,noise}$), which was computed by taking the average of the total signal between the altitudes of 80 and 120 km, where atmospheric backscattering was expected to be negligible. The uncertainty of the calibration coefficient (δK) was estimated as the standard deviation of K, which was obtained from the comparison of uncalibrated ~~RL~~ MRL-derived data with the radiosonde data for the measurement period. As quality control (QC) of the derived data, we excluded data with uncertainty larger than 30% or $w >$ 30 g/kg.

2.4 Calibration coefficient of the water vapor mixing ratio

To obtain the absolute value of w from the lidar signals, the calibration coefficient K of Eq. (1) was first determined as described in Sect. 2.3. However, temporal change in K is a critical problem for long-term operation of the system, because if the temporal variation is large, K must be obtained frequently during the measurement period. We investigated this problem by examining the temporal variation in K values obtained by comparing uncalibrated ~~RL~~ MRL-derived w with collocated radiosonde measurements obtained daily at 20:30 LST from August to December 2016 (Fig. 4). Radiosondes (RS-11G, Meisei Electric. Co., Japan) were launched twice daily (8:30 and 20:30 LST) from an aerological observatory located 80 m northeast of the ~~RL~~ MRL, and, according to the manufacturer, the measurement uncertainty of relative humidity by the RS-11G radiosonde is 5% in the lower troposphere and 7% in the upper troposphere (http://www.meisei.co.jp/english/products/RS-11G_E.pdf). During the test period, the ~~RL~~ MRL system was operated nearly continuously at the Meteorological Research Institute in Tsukuba, except for short interruptions for flash lamp replacement (31 August and 24 October), power outages (18 August and 23 October), and trailer inspection (31 October to 6 November). We calculated K only for the nighttime (20:30 LST) data because at night the ~~RL~~ MRL measurement uncertainty was small between altitudes of 1 and 5 km (see Sect. 3.1). After 12 August, the value of K was nearly constant during the test period: mean ± standard deviation = 52.4 ± 2.1 (Fig. 4). Unfortunately, the reason for the abrupt change in K on 11 August from 57.4 ± 1.5 is unknown because we did not make any changes to the instrument at that time. Nevertheless, given the uncertainty of K (4% in this case), we may say that the ~~RL~~ MRL can be operated for at least 4 months without calibration. The possible reason for the variation of K is the variation of temperature in the trailer that can change the sensitivity of PMTs and center wavelength of IFs. During the experimental period, the variation of temperature in the trailer was at most ± 5 K, which corresponds to <6% variation of the effective Raman backscattering cross section ratio and thus K, assuming that the temperature variation of the sensitivity of PMT is <0.4%/K (Hamamatsu Photonics, 2017) and that of the filter CWL is < 0.0035 nm/K (FUJITOK, Japan, personal communication). To reduce the temperature variations, we need more stringent control of the temperature of the receiving system. We also examined the value of K before the system was moved from Tsukuba to the Tokyo Bay area (110 km or 70 km from Tsukuba) with that obtained after the move, from 15 June to 9 November 2017 (not shown). Before the system was moved, K was 46.9 ± 1.8, and afterward it was 43.1 ± 2.3, a change of 8.6% (we note also that after the telescope focus was readjusted in January 2017, the value of K changed from what it had been in 2016). These results indicate that the calibration coefficient should be determined before and after deployment of the system, and the average and standard deviation of those values should be used for K and δK.

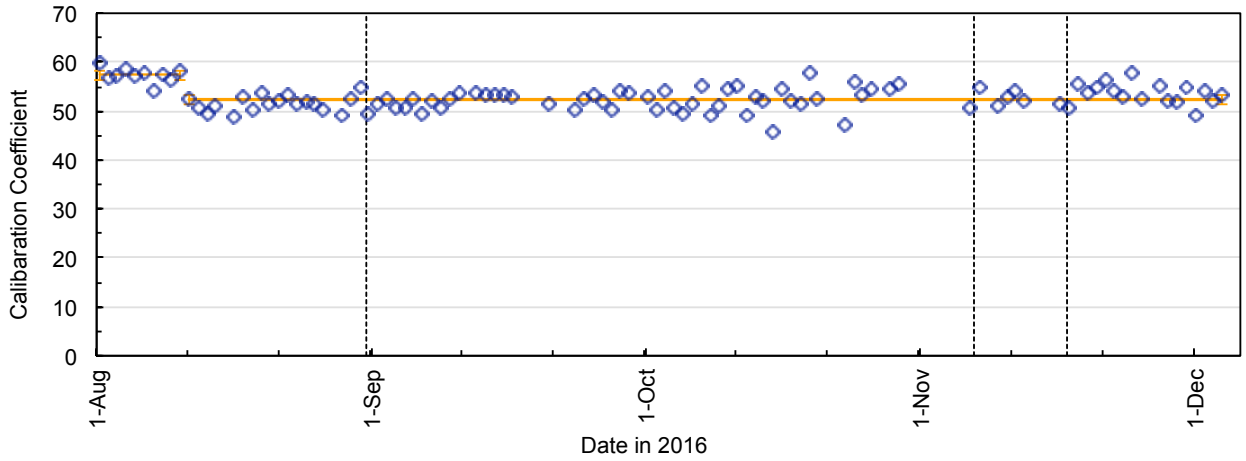

Figure 4. Temporal variation of the calibration coefficient of the water vapor mixing ratio (K) for the ~~mobile RL~~MRL obtained by comparison with collocated radiosonde measurements at 20:30 LST from August to December 2016. The horizontal orange lines show the averages before and after 12 August. The vertical dotted lines indicate dates on which the optical axis was adjusted.

2.5 Beam overlap correction for the Raman channels

Values of w calculated from the ~~RL~~ MRL signals for altitudes below 0.5 km were systematically lower than values obtained with the radiosonde when it was assumed that the beam overlap functions for the Raman water vapor and nitrogen channels were equal (i.e. $\frac{O_{H_2O}(z)}{O_{N_2}(z)} = 1$). When we compared the vertical distribution of the ratio of w obtained by radiosonde to that obtained by the ~~RL~~ MRL without beam overlap correction (Fig. 5), we found considerable variation among individual profiles, but the average value of the ratio increased from 1 to 1.1 with a decrease of altitude from 0.7 to 0.1 km. Possible reasons for the difference in the overlap functions of the two Raman channels at low altitude are the difference in the optical paths (Fig. 1) and the spatial inhomogeneity of PMT sensitivity (Simeonov et al., 1999; Hamamatsu Photonics, 2017). To correct for the difference, we derived the ratio of beam overlap functions by comparing w obtained with the ~~RL~~ MRL under the assumption of $\frac{O_{H_2O}(z)}{O_{N_2}(z)} = 1$ with w obtained by radiosonde. Then, we calculated the mean vertical profile of the ratios and fitted a quadric curve to the profile for use in Eq. (1) to calculate w. The magnitude of the correction increased from 1% at 0.5 km altitude to 8% at 0.1 km. The uncertainty of the correction was estimated to be 8% from the standard deviation of the profiles. The possible reasons for the variation among the profiles are difference of the measurement period and temporal resolution (i.e. 20 minutes average for the lidar and approximately 1 second for the radiosonde), difference of the vertical resolution (i.e. 75 m for the lidar and 20–300 m that depends on the significant pressure level interval for the radiosonde, and lidar noise. The variation should be reduced if using the data measured above the lidar by using a kite (Totems and Chazette, 2016) or unmanned aerial vehicles.

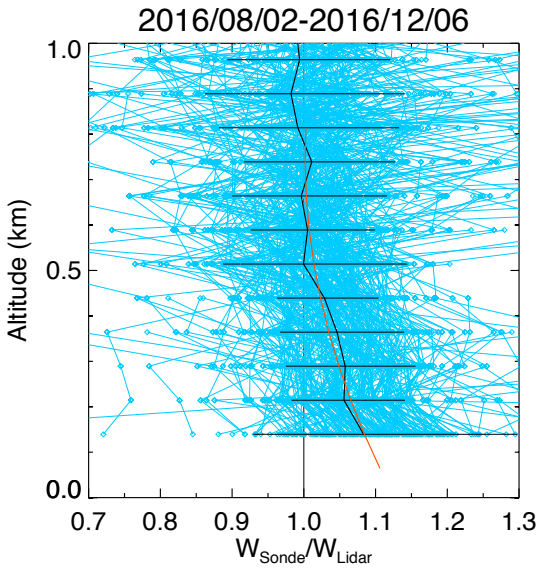

Figure 5. Vertical distribution of the ratio of w obtained by radiosonde (w_{Sonde}) to w obtained with the ~~RL~~ MRL system without beam overlap correction (w_{Lidar}) from 2 August to 6 December 2016. The individual profiles are shown by the thin blue lines with diamonds. The solid black line and the error bars are averages and standard deviations over 75 m height interval. A quadric curve (orange line) was fitted to the averaged values.

3 Validation results

Measurements for validation of the ~~RL~~ MRL system measurements were made on 120 days, from 2 August to 6 December 2016, over Tsukuba, Japan (36.06ºN, 140.12ºE). We validated ~~RL~~ MRL-derived w values (described in Sect. 2.3) by comparing them with radiosonde, GNSS, and high-resolution local analysis (LA) data. A GNSS receiver 80 m west of the ~~RL~~ MRL observed the carrier phase transmitted by GNSS satellites and estimated the precipitable water vapor (PWV) with a temporal resolution of 5 min during the validation period. The PWV value represents the vertically integrated water vapor content averaged over a horizontal distance of approximately 20 km around the antenna. See Shoji et al. (2004) for more details of the derivation method. The LA consists of hourly meteorological data with a horizontal resolution of 2 km over Japan provided by the JMA. These data are obtained by a three-dimensional variational (3D-Var) data assimilation technique from hourly observation data from multiple sources, including surface measurements, satellites, and GNSS-derived PWV data. LA data provide initial conditions to local-scale NWP models used for 9-hour forecasts for aviation, weather warnings and advisories, and very short-range precipitation in and around Japan, provided every hour. The vertical resolution of the LA data is 45–868 m with 48 layers. See JMA (2016) for more details about the LA data.

3.1 Comparison with radiosonde measurements

3.1.1. Vertical distribution

We compared the vertical distribution of w obtained with the ~~RL~~ MRL with w obtained by radiosondes launched at 8:30 and 20:30 LST on 1 September 2016 over Tsukuba (Fig. 6). The ascent speed of the radiosondes was 5–6 m/s, so they reached a height of about 7 km after 20 min. The ~~RL~~ MRL data were accumulated over the 20 min following the radiosonde launch. The vertical resolution is reduced to 75 m below an altitude of 1 km and to 150 m above that to increase the signal-to-noise ratio (SNR) of the Raman backscatter signals. The values of w obtained with the ~~RL~~ MRL agreed well for the altitude range of 0.14–1.7 km with w obtained by radiosonde during 08:30–08:50 LST (Fig. 6a), and they agreed well for altitudes up to 6.2 km with radiosonde measurements made during 20:30–20:50 LST (Fig. 6b). Mean differences were 0.8 g/kg (7%) for the 08:30 LST radiosonde launch and 0.7 g/kg (15%) for the 20:30 LST launch. The maximum height of ~~RL~~ MRL measurements with

an uncertainty of less than 30% was only 1.5 km in the daytime, because solar light reduces the SNR of the Raman backscatter signals; for example, at 08:30 LST on 1 September 2016, the solar zenith angle was 50° (Fig. 6a).

The altitude–time cross section of w obtained with the ~~RL~~ MRL on 1 September 2016 (Fig. 7) showed considerable diurnal moisture variation below an altitude of 3 km. The top height of a moist region (w > 12 g/kg) present below an altitude of 1 km during 00–03 LST increased to above 2 km as the sun rose during 03–06 LST. At midday, the top height of the moist region was probably above 1.5 km (although it cannot be seen because of the low SNR ratio in strong sunlight). After sunset, it remained at an altitude of 2.5 km, which probably corresponded to the top of a residual layer. The top of another moist region with w of 15 g/kg that emerged below an altitude of 1 km after 18 LST undulated with a vertical amplitude of a few hundred meters and a period of ~3 h. This result demonstrates the utility of the ~~RL~~ MRL system for monitoring the diurnal variation of water vapor in the lower troposphere, which is not captured by routine radiosonde measurements.

To test the long-term stability of the ~~mobile RL~~MRL system, we operated it for four months, from 2 August to 6 December 2016. After QC of the ~~RL~~ MRL data, the maximum measurement height was mostly ~1 km during the day throughout the measurement period, whereas at night when low, thick clouds were absent, it decreased from 6 km to 2.5 km over the measurement period (Fig. 8). We attribute this nighttime decrease to 1) a drop by almost half in the power of the laser transmitter during its continuous operation for three months, which caused the SNR of the signals to decrease, and 2) decreases in the water vapor concentration from summer to winter in the lower troposphere, which caused a decrease in the strength of Raman backscatter water vapor signals. As for the laser power, it increased from 110 mJ/pulse to 220 mJ/pulse after replacing the flash lamp and adjusting the angles of second and third harmonic crystals on 8 December 2017. As for the water vapor concentration, the monthly mean w values decreased from 17 to 4 g/kg at 1000 hPa and from 8 to 1 g/kg at 700 hPa between August and December in 2016.

In general, vertical distributions of w obtained with the ~~RL~~ MRL system agreed well with radiosonde measurements (Fig. 9). However, ~~but~~ the ~~RL~~ MRL- and radiosonde-derived values sometimes differed considerably from LA data for the same dates (e.g. between 2.5 and 3.5 km at 20:30 LST on 9 August, between 1.5 and 2.5 km at 20:30 LST on 16 September, and between 0.5 and 1.2 km at 20:30 LST on 2 December 2016) ~~(Fig. 9). These results suggest that the assimilation of RL-derived data can improve the initial conditions of the water vapor distribution in NWP models.~~More detailed analysis will be given in Sect. 3.3.

To study the height dependence of the difference ($w_{\mathrm{Lidar}} - w_{\mathrm{Sonde}}$), we examined the vertical variation of the mean difference at intervals of 500 m (Fig. ~~11~~10). The mean difference was less than 1 g/kg (10%) below an altitude of 6 km at night and below 1 km in the daytime. Above these altitudes, the ~~RL~~ MRL values were higher than the radiosonde-derived values. Possible reasons for the larger differences at higher altitudes are 1) the small number of data points in those regions (Fig. 1~~1~~0d), which caused the statistical significance to be low, 2) the difference in the air parcel measured by the two instruments, because as they ascended the radiosondes were sometimes blown several kilometers or more from the ~~RL~~ MRL position by horizontal winds, particularly above an altitude of 6 km at night, and 3) the generation of spurious Raman signals above 1 km by high solar background radiation in the daytime, as will be discussed in ~~(see~~ Sect. 3.1.2~~)~~.

(a) (b)

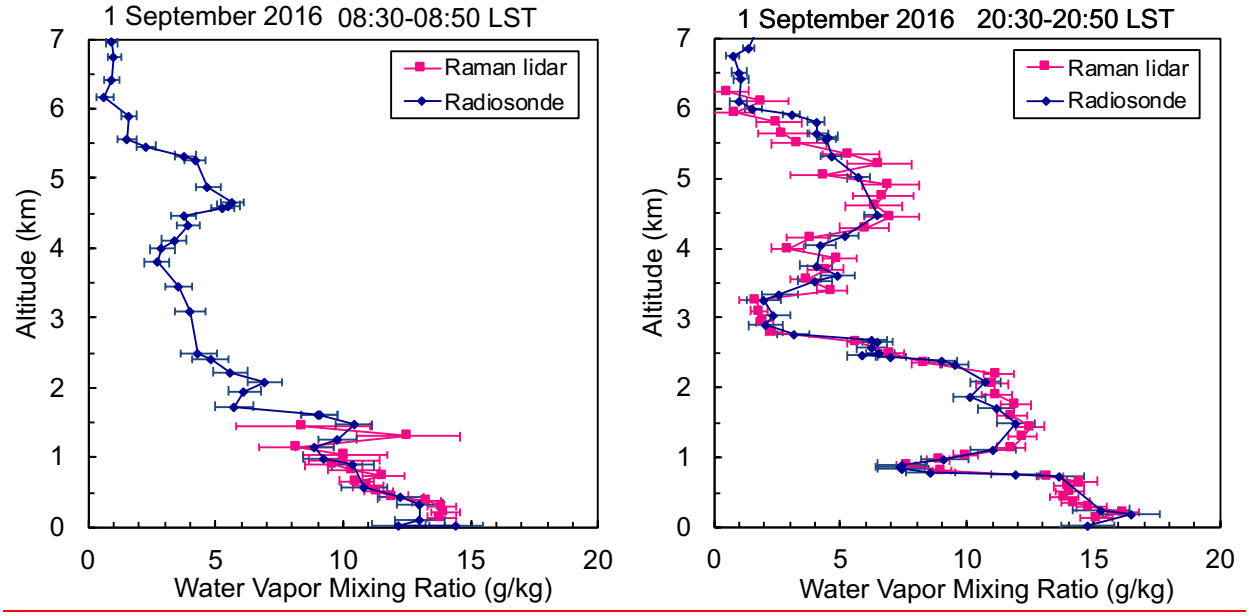

Figure 6. Vertical distributions of the water vapor mixing ratio obtained with the ~~mobile RL~~MRL (magenta), radiosonde (dark blue) on 1 September 2016 over Tsukuba. The measurement periods for the ~~RL~~ MRL were (a) 08:30–08:50 and (b) 20:30–20:50 LST, and the radiosondes were launched at (a) 8:30 LST and (b) 20:30 LST. ~~RL~~ MRL data with uncertainty of less than 30% are plotted.

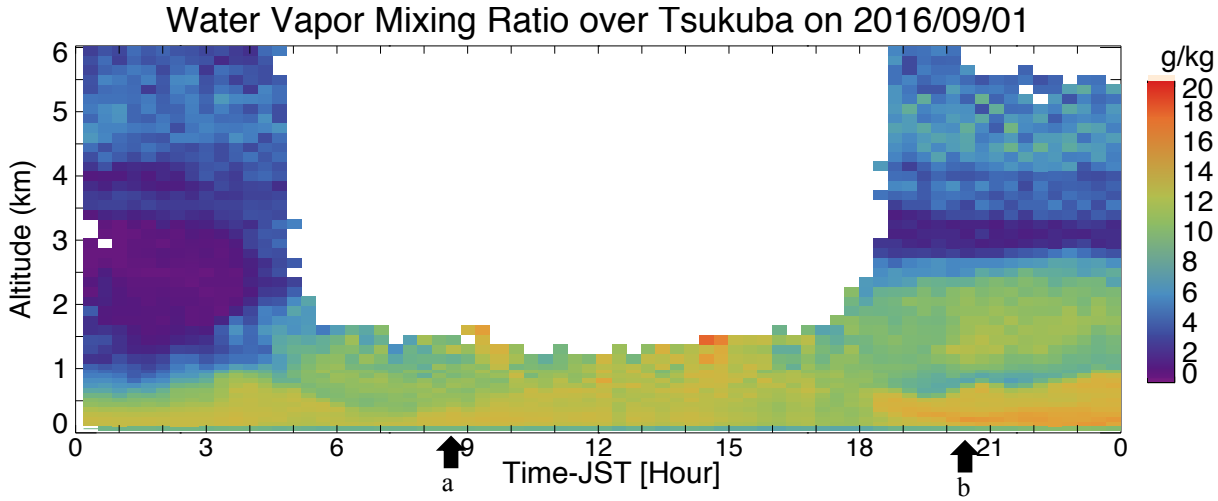

Figure 7. Altitude–time cross section of water vapor mixing ratios obtained with the ~~mobile RL~~MRL on 1 September 2016. Data with uncertainty of less than 30% are plotted. Arrows at the bottom show the start of the measurement periods for the data shown in Fig. 6.

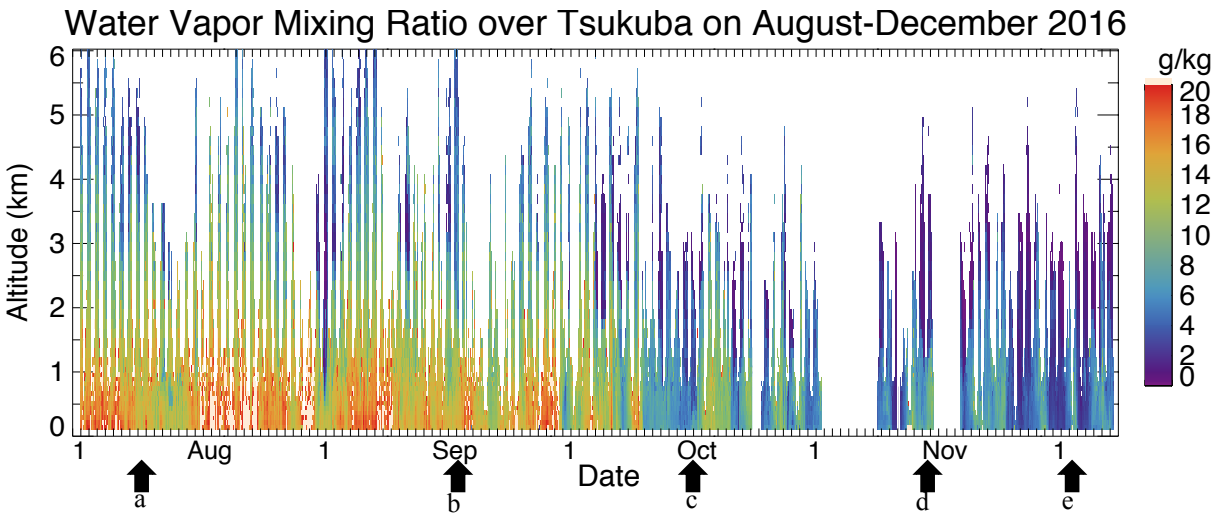

Figure 8. Altitude–time cross section of water vapor mixing ratios obtained with the ~~mobile RL~~MRL from 2 August to 6 December 2016. Data with uncertainty of less than 30% are plotted. Arrows at the bottom show the dates for which vertical profiles are shown in Fig. 9.

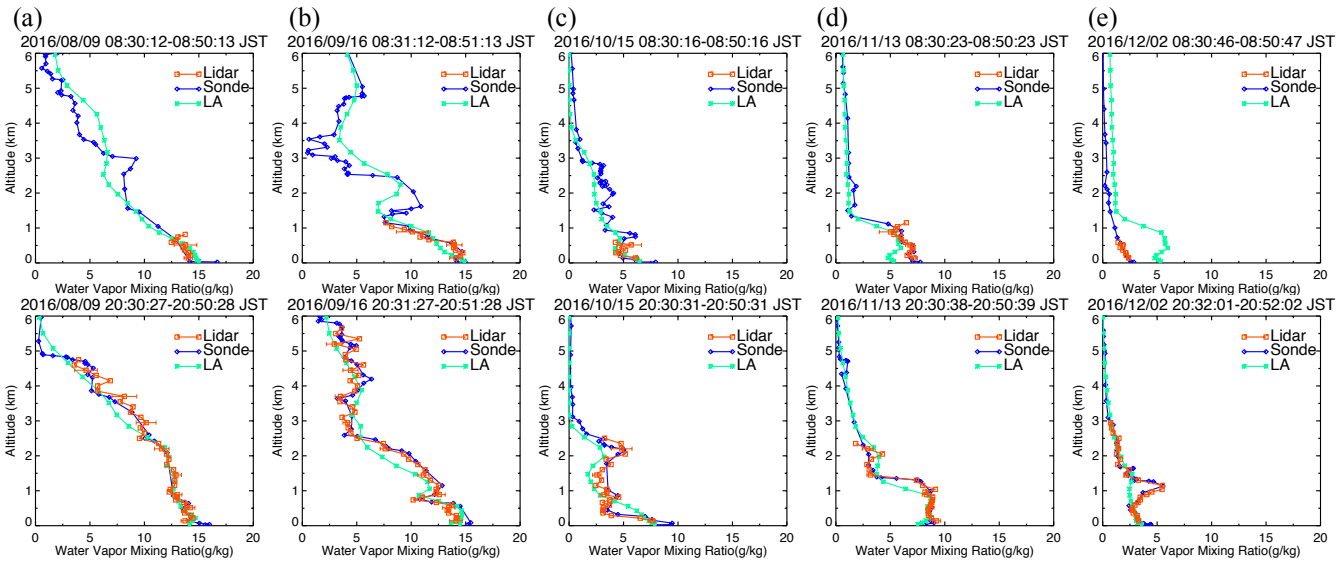

Figure 9. Vertical distributions of water vapor mixing ratios obtained with the ~~mobile~~ MRL (orange) and radiosondes (blue) compared with local analysis data (green) for 08:30 LST (upper panel) and 20:30 LST (bottom panels) on (a) 9 August, (b) 16 September, (c) 15 October, (d) 13 November, and (e) 2 December 2016.

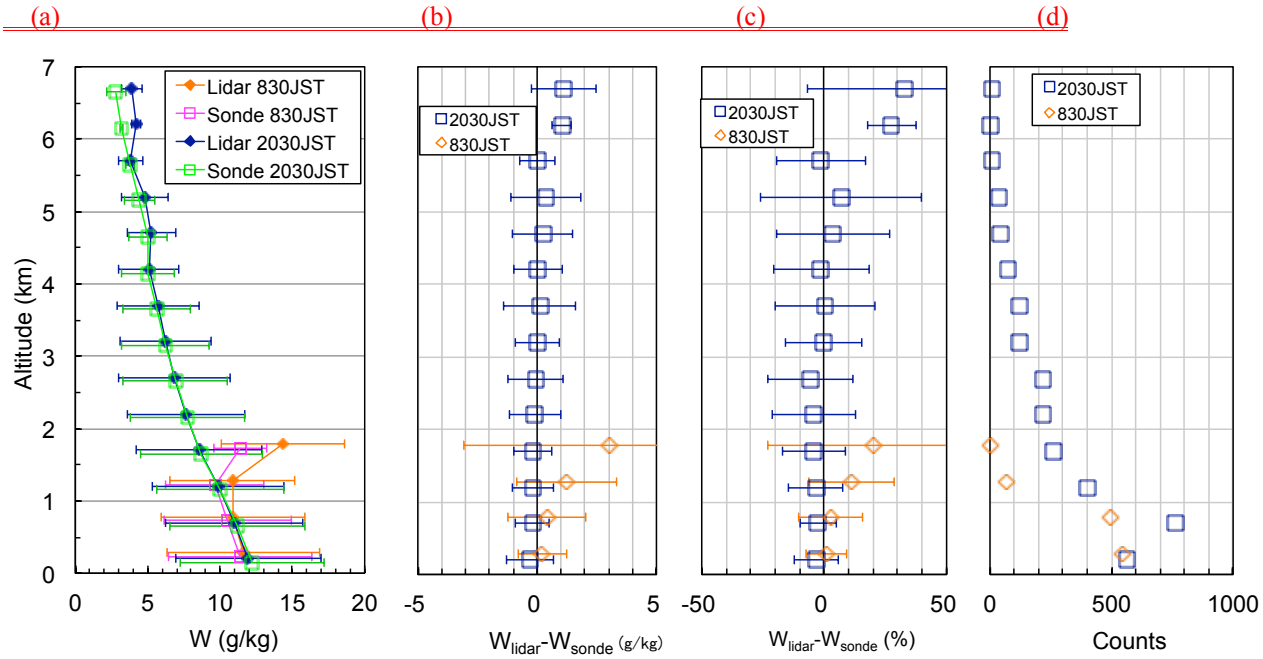

Figure 1~~1~~0. Vertical variations of (a) mean w_{Lidar} values (diamonds) and w_{Sonde} (open squares) values at intervals of 500 m for 20:30 LST and 08:30 LST from 2 August to 6 December 2016, and their (b) absolute and (c) relative differences. Symbols and error bars in (a)–(c) show means and standard deviations. (d) The number of data points at each altitude.

3.1.2 Scatter plot comparison

After the data were screened for QC, we compared w values obtained with the ~~RL~~ MRL and by radiosonde from 2 August to 6 December 2016 in 110 vertical profiles for 20:30 LST and 113 for 08:30 LST (Fig. ~~10~~11). For this comparison, the radiosonde data were linearly interpolated to the heights of the ~~RL~~ MRL data. Note that the maximum altitude of the comparison for 08:30 LST (1.9 km) was lower than that for 20:30 LST (6.85 km) because, owing to their large uncertainty, daytime data at higher altitudes were excluded by the QC screening. The ~~RL~~ MRL-derived w (w_{Lidar}) values agreed with the radiosonde-derived values (w_{Sonde}) over the range from 0 to 20 g/kg (Fig. ~~10~~11). A geometric mean regression analysis conducted by assuming that w_{Sonde} = slope × w_{Lidar} + bias yielded a slope of 0.990 and an intercept of –0.002 for the 20:30 LST (Fig. ~~10a~~11a) and a slope of 1.045 and an intercept of –0.005 g/kg for 08:30 LST (Fig. ~~10b~~11b). To examine the dependence of the difference in w ($w_{Lidar} - w_{Sonde}$) on the magnitude of w_{Sonde}, we plotted ($w_{Lidar} - w_{Sonde}$) as a function of w_{Sonde}, as well as the means and standard deviations of ($w_{Lidar} - w_{sonde}$), at intervals of 2.5 g/kg (Figs. ~~10c~~ 11c and ~~10d~~11d). As a result, we found no significant bias in the difference ~~– w_{sonde} relationship~~ for w_{Sonde} ranging from less than 20 g/kg at night to less than 15 g/kg in the daytime (i.e., mean differences were smaller than 0.3 g/kg). In contrast, we found positive biases for larger w_{Sonde} value ranges; the bias was 1.7 g/kg at 08:30 LST for w ranging from 17.5 to 20 g/kg. A possible reason for the daytime bias at high values of w_{Sonde} is that high solar background radiation generated spurious noise spikes and high photon counts in Raman water vapor signals above an altitude of 1 km that were not rejected by QC. We are investigating the method to reject such data by QC, although they have small impacts on the water vapor fields analyzed from the data assimilation because their measurement errors are large.

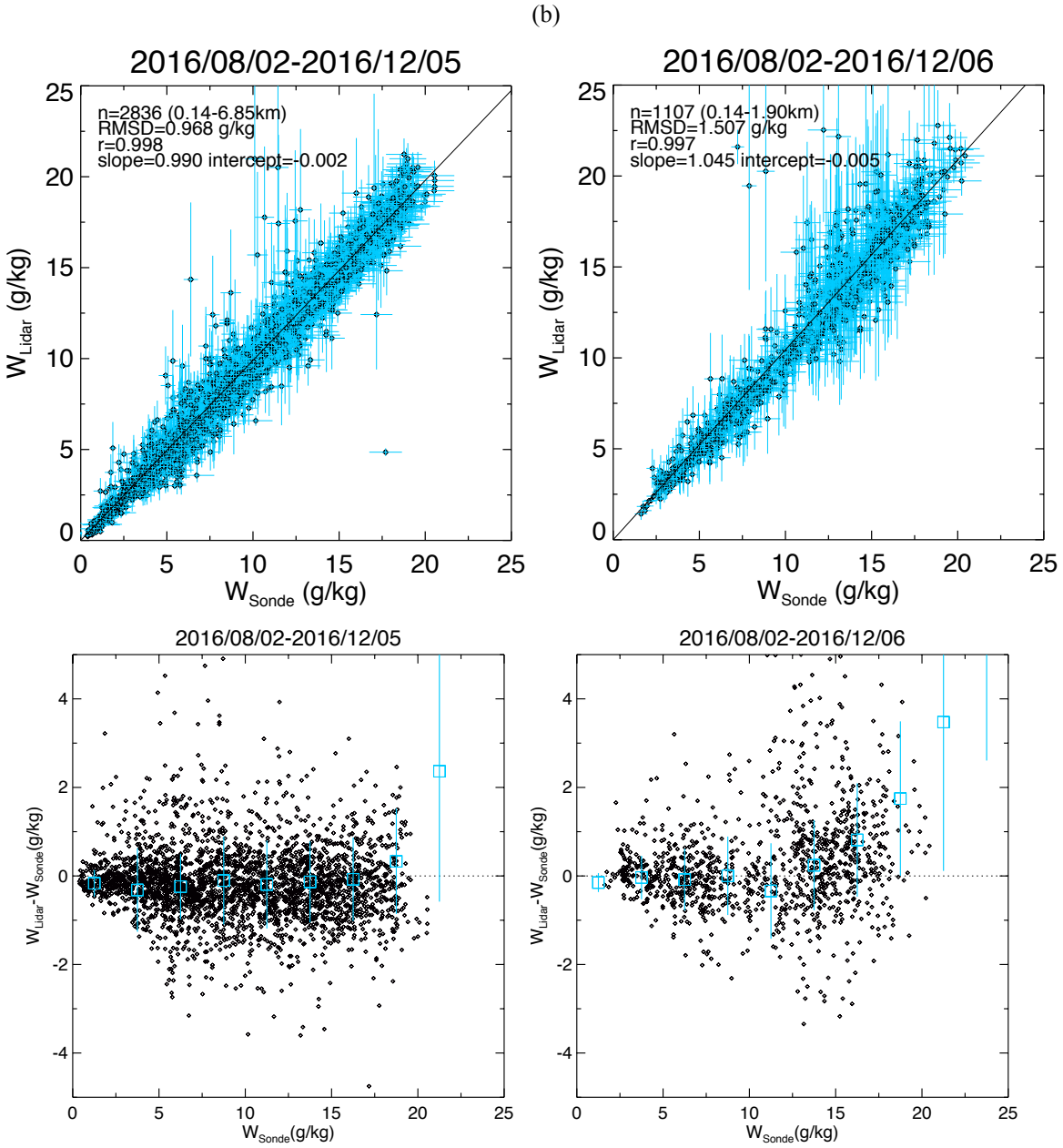

Figure ~~10~~11. (Top panels) Scatter plots of w obtained with the ~~RL~~ MRL (w_{Lidar}) versus w obtained with radiosondes (w_{Sonde}) at (a) 20:30 LST and (b) 08:30 LST from 2 August to 6 December 2016. (Bottom panels) Scatter plots of the difference ($w_{Lidar} - w_{Sonde}$) as a function of w_{Sonde} at (c) 20:30 LST and (d) 08:30 LST. Blue symbols show the means, and the blue lines show the standard deviations of the difference at intervals of 2.5 g/kg. Data points with an ~~RL~~ MRL measurement uncertainty of less than 30% are plotted.

~~3.1.3 Vertical distribution comparison~~

~~To study the height dependence of the difference ($w_{Lidar} - w_{Sonde}$), we examined the vertical variation of the mean difference at intervals of 500 m (Fig. 11). The mean difference was less than 1 g/kg (10%) below an altitude of 6 km at night and below 1 km in the daytime. Above these altitudes, the RL values were higher than the radiosonde-derived values. Possible reasons for the larger differences at higher altitudes are 1) the small number of data points in those regions (Fig. 11d), which caused the statistical significance to be low, 2) the difference in the air parcel measured by the two instruments, because as they ascended the radiosondes were sometimes blown several kilometers or more from the RL position by horizontal winds, particularly above an altitude of 6 km at night, and 3) the generation of spurious Raman signals above 1 km by high solar background radiation in the daytime (see Sect. 3.1.2).~~

~~(a) (b) (c) (d)~~

~~**Figure 11.** Vertical variations of (a) mean w_{Lidar} values (diamonds) and w_{Sonde} (open squares) values at intervals of 500 m for 20:30 LST and 08:30 LST from 2 August to 6 December 2016, and their (b) absolute and (c) relative differences. Symbols and error bars in (a)–(c) show means and standard deviations. (d) The number of data points at each altitude.~~

3.2 Comparison with GNSS PWV data

To validate the ~~RL~~ MRL measurement data for times when coincident radiosonde data were unavailable, we compared the ~~RL~~ MRL-derived PWV with PWV values obtained from GNSS data. To obtain PWV from the ~~RL~~ MRL data, we computed the vertical profile of the water vapor density from ~~RL~~ MRL-derived w and atmospheric density obtained by the radiosonde closest in time to the ~~RL~~ MRL measurement period, and vertically integrated the water vapor density from an altitude of 0.14 km to the maximum height with a measurement uncertainty of less than 30%. Below 0.14 km, we interpolated the ~~assumed that the value of~~ w data to the ground level in-situ measurement~~was the same as that at 0.14 km~~. Then we compared the temporal variations of PWV obtained with the ~~RL~~ MRL with those obtained from GNSS data from August to December 2016 (Fig. 12). So that this comparison would be meaningful, we excluded ~~RL~~ MRL data obtained when the maximum measurement height was lower than 5 km; as a result, mostly nighttime lidar values obtained when low, thick clouds were absent were used in the comparison. The temporal resolution of the GNSS data was reduced by averaging from 5 min (original GNSS resolution) to 20 min to match the resolution of the ~~RL~~ MRL data.

The temporal variation of ~~RL~~ MRL-derived PWV was similar to that of the GNSS-derived PWV (Fig. 12). In summer (August–September), when a moist air mass from the Pacific Ocean covered the observation area, the PWV values were mostly higher than 30 mm. In autumn and winter (October–December), when a dry air mass from the Asian continent prevailed, the PWV values were mostly lower than 20 mm. We note that the number of available lidar PWV data was smaller in autumn and winter than in summer because the decrease in the laser power as mentioned before (Sect. 3.1.1) and because in autumn and winter the Raman backscatter signal tends to be weak by the low water vapor concentration in the middle troposphere. The regression analysis of PWV derived from ~~RL~~ MRL data against GNSS-derived PWV showed a strong positive correlation (correlation coefficient 0.~~990~~991; Fig. 13a) between them, but many of the ~~RL~~ MRL-derived PWV values were lower, most by up to 5 mm, than the GNSS-derived values (Fig. 13b). The most plausible reason for the lower ~~RL~~ MRL-derived PWV values is that the ~~RL~~ MRL did not always measure the entire water vapor column. In addition, both positive and negative differences could be caused by the measured air masses being different (see Sect. 3). The difference in PWV would be large if large horizontal inhomogeneity of the water vapor concentration existed in the observation area. Shoji et al. (2015) utilized the slant path delay of the GNSS signal to estimate the horizontal inhomogeneity of water vapor on a scale of several kilometers around the measurement site. The use of a technique that combines ~~RL~~ MRL and GNSS observations for monitoring the vertical and horizontal distributions of water vapor holds promise, and the development of such a technique is our future task.

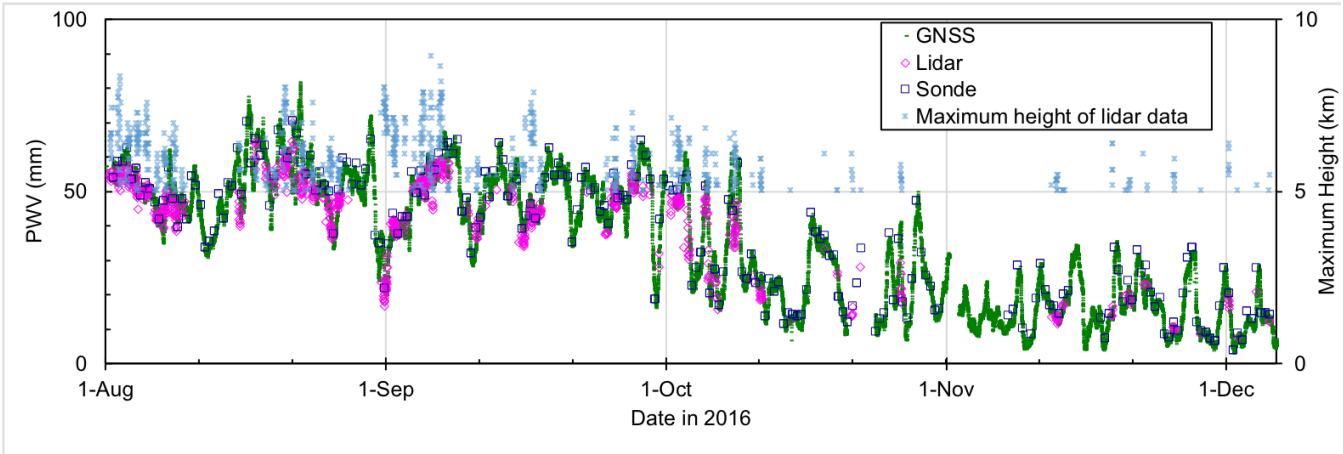

Figure 12. Temporal variations of PWV obtained with lidar (magenta diamonds), GNSS (green dots), and radiosonde (blue squares) from 2 August to 6 December 2016 over Tsukuba. Data with measurement uncertainties of less than 10% that were obtained when the maximum ~~RL~~ MRL measurement height exceeded 5 km (light blue asterisks) are plotted.

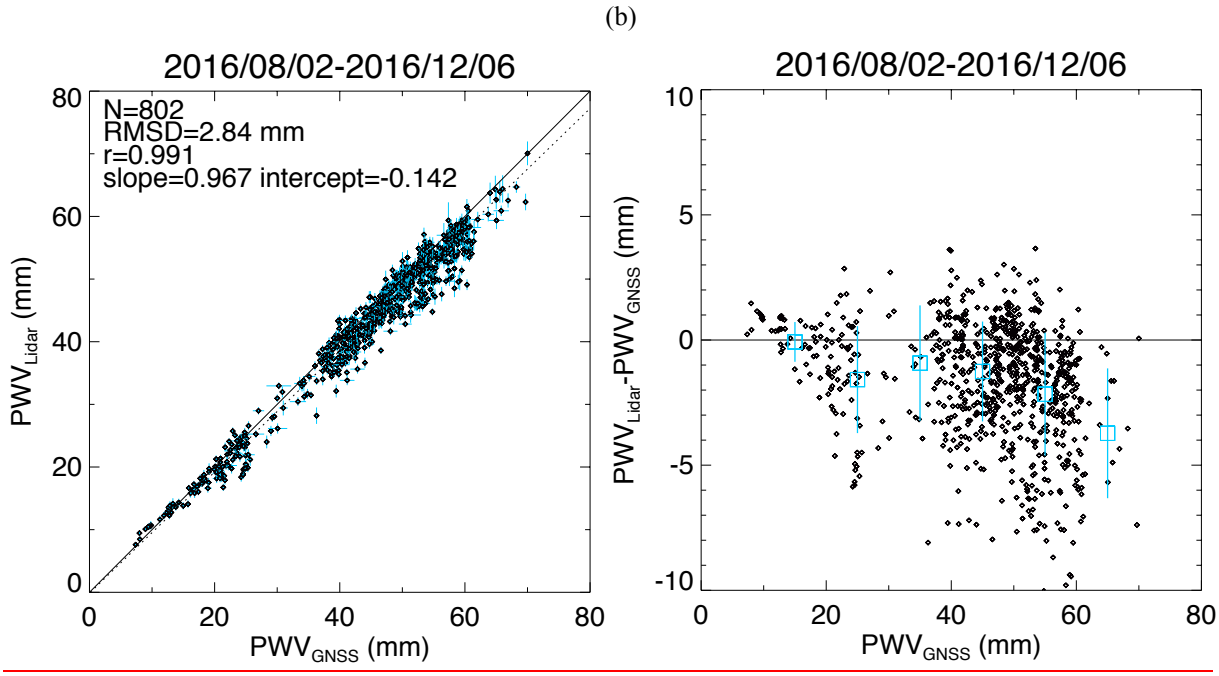

Figure 13. Scatter plots (a) of PWV obtained with the ~~mobile RL~~MRL system against PWV obtained from GNSS data from 2 August to 6 December 2016 and (b) their difference ($PWV_{Lidar} - PWV_{GNSS}$) versus PWV_{GNSS}. In (b), the open squares and vertical lines show the means and standard deviations of the difference at intervals of 10 mm.

3.3 Comparison with local analysis data

~~**3.3.1 Scatter plot comparison**~~

~~We compared hourly RL values of w with LA data because the primary purpose of our RL measurement was to improve the initial condition of the water vapor field of the NWP model (Fig. 14). For this comparison, the RL data were linearly interpolated to the heights of the LA data. The result revealed that the root mean square difference (RMSD) (1.367 g/kg) was larger than that obtained when we compared RL values with nighttime radiosonde values (0.968 g/kg; Fig. 10a). Moreover, the RL-derived w values were consistently higher, by 0.2–0.8 g/kg (1–11%), than those derived by LA for w in the range of 0–22.5 g/kg (Fig. 14b). We also compared LA data with the radiosonde data for the same period (not shown) and found that the mean LA data at intervals of 2.5 g/kg differed from the radiosonde data by −0.2 to 0.9 g/kg (3–11%). We infer that the LA data used in this comparison had a negative bias because the accuracy of the radiosonde relative humidity measurements was 5–7%.~~

~~3.3.2~~ 3.3.1 Vertical distributions

We compared hourly MRL values of w with LA data because the primary purpose of our MRL measurement was to improve the initial condition of the water vapor field of the NWP model. Our comparison of vertical variations in w obtained with the ~~RL~~ MRL system with w derived from the LA (Fig. 9) showed the higher values of the MRL than the LA data. The statistics of the comparison showed that the ~~RL~~ MRL values were higher by up to 1.1 g/kg (25%) over the entire altitude range (Fig. 15). In addition, the magnitude of the difference ($w_{Lidar} - w_{LA}$) was larger than the difference with radiosonde values ($w_{Lidar} - w_{Sonde}$) (Fig. ~~11~~10). This result suggests that the assimilation of ~~RL~~ MRL data has the potential to improve the initial conditions provided to the NWP model.

3.3.~~1~~2 Scatter plot comparison

Figure 14 shows the scatter plot of w obtained with MRL ~~We compared hourly RL values of *w* with LA data because the primary purpose of our RL measurement was to improve the initial condition of the water vapor field of the NWP model (Fig. 14).~~ For this comparison, the ~~RL~~ MRL data were linearly interpolated to the heights of the LA data. The result revealed that the root mean square difference (RMSD) (1.367 g/kg) was larger than that obtained when we compared ~~RL~~ MRL values with nighttime radiosonde values (0.968 g/kg; Fig. 1~~0~~1a). Moreover, the ~~RL~~ MRL-derived *w* values were consistently higher, by 0.2–0.8 g/kg (1–11%), than those derived by LA for *w* in the range of 0–22.5 g/kg (Fig. 14b). We also compared LA data with the radiosonde data for the same period (not shown) and found that the mean LA data at intervals of 2.5 g/kg differed from the radiosonde data by –0.2 to 0.9 g/kg (3–11%). We infer that the LA data used in this comparison had a negative bias because the accuracy of the radiosonde relative humidity measurements was 5–7%. The differences with the LA data can be related to local effects and thus to the representativeness of the measurement site at the mesoscale. They can also be due to a problem in the assimilation process if it does not integrate well the error matrices.

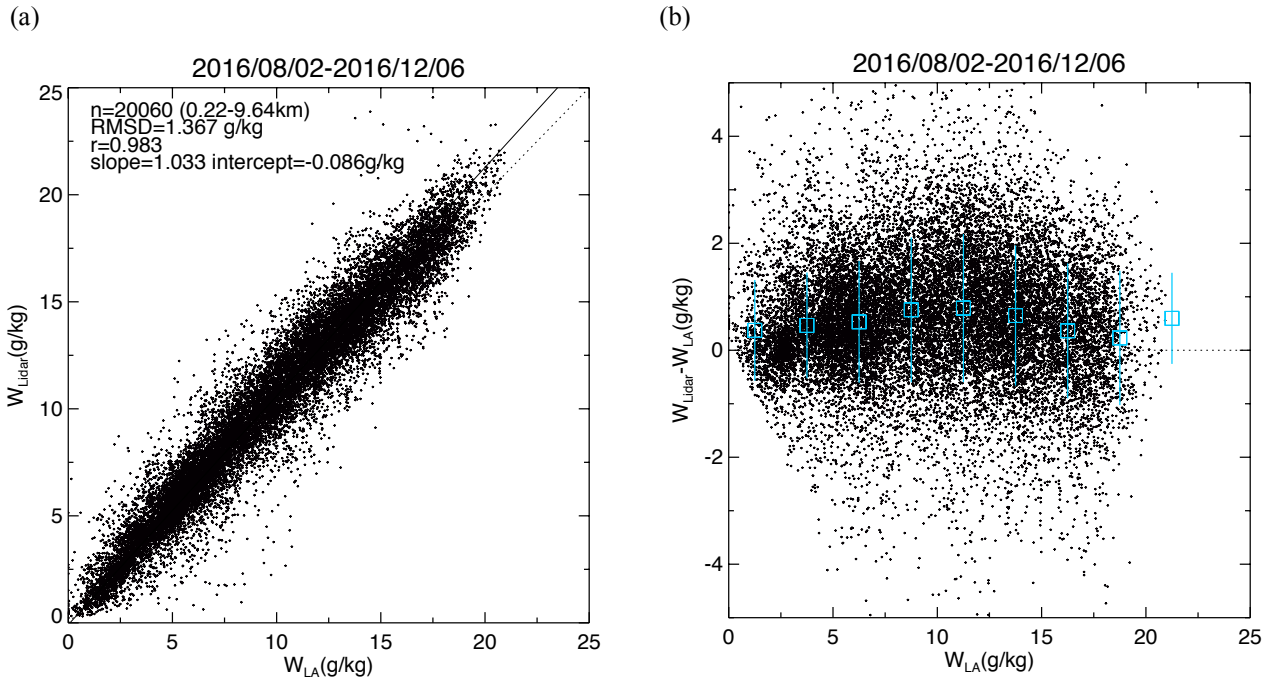

Figure 14. Scatter plots of (a) w obtained with the ~~RL~~ MRL (w_{Lidar}) versus w obtained from the local analysis (w_{LA}) and (b) their difference ($w_{\mathrm{Lidar}} - w_{\mathrm{LA}}$) as a function of w_{LA} from 2 August to 6 December 2016. In (b), the blue open squares and vertical lines show means and standard deviations of the difference at intervals of 2.5 g/kg.

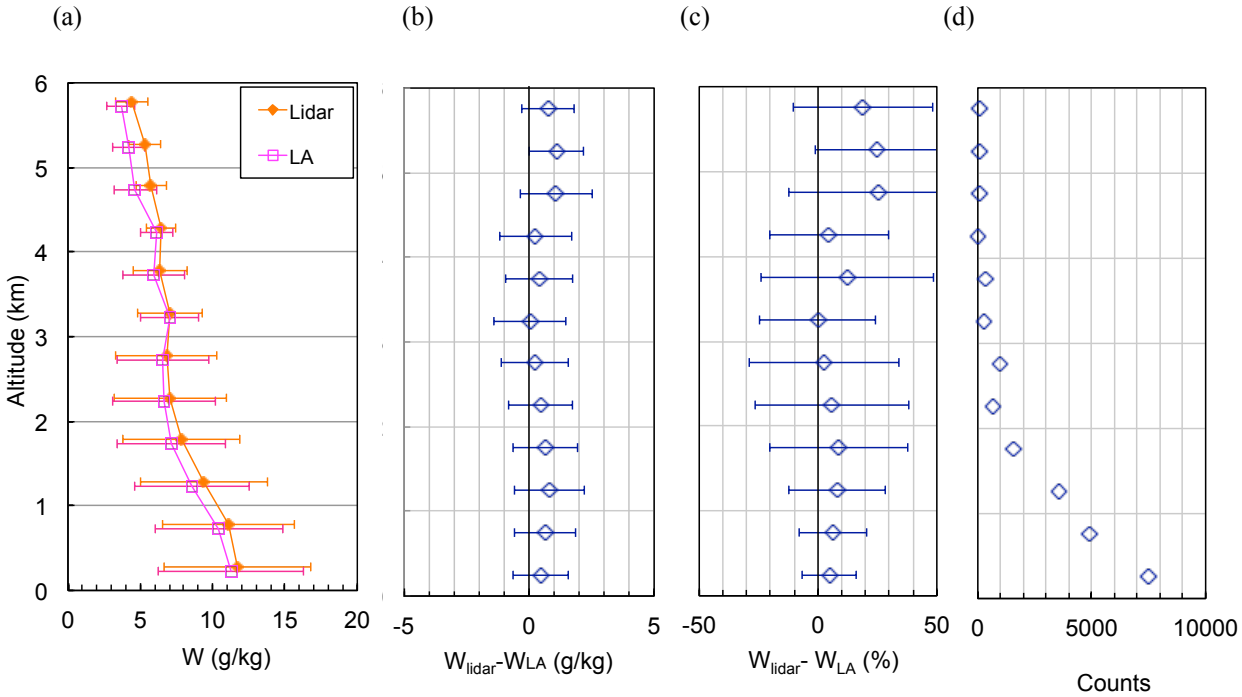

Figure 15. Vertical variations of (a) mean values and standard deviations of w obtained with the ~~RL~~ MRL (w_{Lidar}) and from the local analysis (w_{LA}) at 500-m intervals and their (b) absolute and (c) relative differences from 2 August to 6 December 2016. Symbols and error bars in (b) and (c) show the means and standard deviations of the difference. (d) The number of data points at each altitude.

3.4 Summary of the validation results and outlook

Table 3 summarizes the results of our comparisons of water vapor measurements obtained by the ~~RL~~ MRL and other instruments or local analyses. The correlation was highest and the RMSD was smallest when ~~RL~~ MRL-derived *w* was compared with *w* obtained by radiosonde at night. This result was probably because 1) the ~~RL~~ MRL system was calibrated by using radiosonde data, 2) the instruments measured the same quantity (*w*), and 3) the measurement performance of the ~~RL~~ MRL was best at night. The agreement with radiosonde data was not as good in the daytime as it was at night because of the measurement uncertainty of *w* was larger in the daytime, even though the slope and intercept of the regression analysis did not differ significantly between daytime and nighttime measurements. The ~~RL~~ MRL-derived PWVs at night were slightly lower than those derived from GNSS data because of the measurement range limitation of the ~~RL~~ MRL system. The regression analysis of ~~RL~~ MRL-derived *w* versus LA data showed that the magnitudes of the deviation of the slope from 1 and the deviation of the intercept from zero were larger than those obtained in the analysis with radiosonde data, and the correlation coefficient was the lowest among the comparisons. From these results, we can conclude that assimilation of ~~RL~~ MRL-derived *w* after QC can improve the initial conditions of the NWP model for heavy rain forecasting.

A first data assimilation experiment of the MRL-derived vertical profiles of *w* into the JMA-NHM using the three-dimensional LETKF for the heavy rainfall forecasting has been reported by Yoshida et al. (2018a), who showed a positive impact on the analyzed and forecast humidity fields on the Kanto Plain on 17 August 2016. More detailed description of the assimilation experiments will follow soon (Yoshida et al. 2018b). We will increase the cases of the assimilation experiments using the MRL-derived data and evaluate the statistical impact on the heavy rainfall forecast.

Table 3. Results of water vapor measurements by the ~~mobile RL~~MRL compared with data obtained by other instruments or from local analyses.

Data type	Time (LST)	Slope	Intercept (g/kg)	Correlation coefficient	RMSD (g/kg)	No. of data points
Radiosonde	20:30	0.990	–0.002	0.998	0.968	2836
	08:30	1.045	–0.005	0.997	1.507	1107
	All	1.003	–0.001	0.997	0.983	4903
GNSS (PWV)	0:00–23:00	0.~~968~~967	–0.~~229~~142 mm	0.991	2.8~~4~~4 mm	~~836~~802
LA	00:00–23:00 (hourly)	1.033	–0.086	0.983	1.367	20060

~~5~~4 Conclusion

We developed a mobile Raman lidar system for measuring the vertical distribution of the water vapor mixing ratio *w* in the lower troposphere to improve the accuracy and lead time of heavy rainfall prediction. The ~~RL~~ MRL can be easily deployed to remote sites and is capable of unattended operation for several months. Our comparison of the ~~RL~~ MRL-derived *w* values with those obtained with collocated radiosondes showed that they agreed within 10% and RMSD with 0.98 g/kg between altitudes of 0.14 and 5–6 km at night and between altitudes of 0.14 and 1.5 km in the daytime. The calibration coefficient of the ~~RL~~ MRL showed no significant temporal variation during 4 months of continuous operation in 2016. A small correction for beam overlap was necessary below 0.5 km. The ~~RL~~ MRL-derived precipitable water vapor values obtained at night when low clouds were absent and the maximum heights of the ~~RL~~ MRL measurement exceeded 5 km were slightly lower than those obtained from GNSS data. The fact that the ~~RL~~ MRL-derived *w* values were at most 1 g/kg (25%) larger than those in the local analysis

data suggests that assimilation of the ~~RL~~ MRL data can improve the initial condition of the water vapor distribution in the lower troposphere of the NWP model.

The impact of using the lidar data with the nonhydrostatic mesoscale model for simulating heavy rainfall in the Kanto area in summer 2016 reported by Yoshida et al. (2018a) showed a positive impact on the humidity fields that were analyzed and forecasted by the model.

The measurement altitude of the current Raman lidar system is limited to 1.5 km in the daytime. Although this limitation might not preclude the use of data from the system for heavy rain forecasting, it would be better to expand the measurement height range because the mixed layer, where the inflow of the large amount of water vapor that causes heavy rain mostly occurs, can be as high as 2 km. Moreover, humidity in the middle troposphere affects the development of cumulus convections to the upper troposphere. To detect water vapor in the middle troposphere in the daytime, a diode laser-based differential absorption lidar might be useful because it can continuously measure the water vapor concentration up to an altitude of 3 km both in the daytime and at night (Repasky et al., 2013; Spuler et al., 2015). We are also developing such a system (Pham Le Hoai et al., 2016) to improve the model forecast skill for heavy rainfall in urban areas.

Acknowledgements

We used radiosonde data measured by the Japan Meteorological Agency (downloaded from http://www.data.jma.go.jp/obd/stats/etrn/upper/index.php).

References

Bucholtz, A., : Rayleigh-scattering calculations for the terrestrial atmosphere, Appl. Opt., 34, 2765-2773, 1995

Chazette, P., Marnas, F., and Totems, J.: The mobile water vapor aerosol Raman LIdar and its implication in the framework of the HyMeX and ChArMEx programs: application to a dust transport process, Atmos. Meas. Tech., 7, 1629-1647, https://doi.org/10.5194/amt-7-1629-2014, 2014.

Dinoev, T., Simeonov, V., Arshinov, Y., Bobrovnikov, S., Ristori, P., Calpini, B., Parlange, M., and van den Bergh, H.: Raman Lidar for Meteorological Observations, RALMO – Part 1: Instrument description, Atmos. Meas. Tech., 6, 1329-1346, https://doi.org/10.5194/amt-6-1329-2013, 2013.

Engelmann, R., Kanitz, T., Baars, H., Heese, B., Althausen, D., Skupin, A., Wandinger, U., Komppula, M., Stachlewska, I. S., Amiridis, V., Marinou, E., Mattis, I., Linné, H., and Ansmann, A.: The automated multiwavelength Raman polarization and water-vapor lidar PollyXT: the neXT generation, Atmos. Meas. Tech., 9, 1767-1784, https://doi.org/10.5194/amt-9-1767-2016, 2016.

Goldsmith, J. E. M., F. H. Blair, S. E. Bisson, and D. D. Turner: Turn-key Raman lidar for profiling atmospheric water vapor, clouds, and aerosols, Appl. Opt., 37, 4979-4990, 1998.

Japan Meteorological Agency (JMA), Climate change monitoring Report 2016, 93pp., downloaded from http://www.jma.go.jp/jma/en/NMHS/indexe_ccmr.html, 2017.

Hamamatsu Photonics, Photomultiplier Tube Handbook, 3rd Ed., p59-62, downloaded from http://www.hamamatsu.com/resources/pdf/etd/PMT_handbook_v3aE.pdf, 2017.

Kato, T., Representative Height of the Low-Level Water Vapor Field for Examining the Initiation of Moist Convection Leading to Heavy Rainfall in East Asia. J. Meteor. Soc. Japan, 82, 69–83, https://doi.org/10.2151/jmsj.2018-008, ~~2014~~2018.

Kunii, M.: Mesoscale data assimilation for a local severe rainfall Event with the NHM–LETKF System. Wea. Forecasting, 29, 1093–1105, https://doi.org/10.1175/WAF-D-13-00032.1, 2014.

Leblanc, T., McDermid, I. S., and Walsh, T. D.: Ground-based water vapor Raman lidar measurements up to the upper troposphere and lower stratosphere for long-term monitoring, Atmos. Meas. Tech., 5, 17-36, https://doi.org/10.5194/amt-5-17-2012, 2012.

Melfi, S. H., J. D. Lawrence, M. P. McCormick: Observation of Raman scattering by water vapor in the atmosphere, Appl. Phys. Lett., 15, 295–297, 1969.

Phong Pham Le Hoai, M. Abo, T. Sakai: Development of field-deployable Diode-laser-based water vapor DIAL, EPJ Web of Conferences 119 05011, doi: 10.1051/epjconf/20161190501, 2016.

Reichardt, J., U. Wandinger, V. Klein, I. Mattis, B. Hilber, and R. Begbie: RAMSES: German Meteorological Service autonomous Raman lidar for water vapor, temperature, aerosol, and cloud measurements, Appl. Opt., 51, 8111-8131, 2012.

Repasky, K.S., Moen, D., Spuler, S., Nehrir, A.R., Carlsten, J.L.: Progress towards an autonomous field deployable diode-laser-based differential absorption lidar (DIAL) for profiling water vapor in the lower troposphere. Remote Sens., 5, 6241-6259, 2013.

Saito, K., J. Ishida, K. Aranami, T. Hara, T. Segawa, M. Narita and Y. Honda: Nonhydrostatic atmospheric models and operational development at JMA. J. Meteor. Soc. Japan, 85B, 271-304, 2007.

Sakai, T., T. Nagai, M. Nakazato, T. Matsumura, N. Orikasa, and Y. Shoji: Comparisons of Raman lidar measurements of tropospheric water vapor profiles with radiosondes, hygrometers on the meteorological observation tower, and GPS at Tsukuba, Japan. J. Atmos. Oceanic Technol., 24, 1407–1423, https://doi.org/10.1175/JTECH2056.1, 2007.

Shoji, Y., and Coauthors: Tsukuba GPS dense net campaign observation: Improvement of GPS analysis of slant path delay by stacking one-way post fit phase residuals. J. Meteor. Soc. Japan, 82, 301–314, 2004.

Shoji, Y., W. Mashiko, H. Yamauchi, and E. Sato: Estimation of local-scale precipitable water vapor distribution around each GNSS station using slant path delay: Evaluation of a tornado case using high-resolution NHM. SOLA, 11, 31–35, doi:https://doi.org/10.2151/sola.2015-008, 2015.

Simeonov, V., G. Larcheveque, P. Quaglia, H. van den Bergh, and B. Calpini: Influence of the photomultiplier tube spatial uniformity on lidar signals, Appl. Opt., 38, 5186-5190, 1999.

Spuler, S. M., Repasky, K. S., Morley, B., Moen, D., Hayman, M., and Nehrir, A. R.: Field-deployable diode-laser-based differential absorption lidar (DIAL) for profiling water vapor, Atmos. Meas. Tech., 8, 1073-1087, https://doi.org/10.5194/amt-8-1073-2015, 2015.

Totems, J. and Chazette, P.: Calibration of a water vapour Raman lidar with a kite-based humidity sensor, Atmos. Meas. Tech., 9, 1083-1094, https://doi.org/10.5194/amt-9-1083-2016, 2016.

Turner, D.D., J.E. Goldsmith, and R. A. Ferrare: Development and Applications of the ARM Raman Lidar, Meteorological Monographs, 57, 18.1–18.15, https://doi.org/10.1175/AMSMONOGRAPHS-D-15-0026.1, 2016.

Whiteman, D. N., S. H. Melfi, and R. A. Ferrare: Raman lidar system for the measurement of water vapor and aerosols in the Earth's atmosphere," Appl. Opt. 31, 3068-3082, 1992.

Whiteman, D. N.: Examination of the traditional Raman lidar technique. I. Evaluating the temperature-dependent lidar equations. Appl. Opt. 42, 2571–2592, 2003.

Whiteman, D. N., Cadirola, M., Venable, D., Calhoun, M., Miloshevich, L., Vermeesch, K., Twigg, L., Dirisu, A., Hurst, D., Hall, E., Jordan, A., and Vömel, H.: Correction technique for Raman water vapor lidar signal-dependent bias and suitability for water vapor trend monitoring in the upper troposphere, Atmos. Meas. Tech., 5, 2893-2916, https://doi.org/10.5194/amt-5-2893-2012, 2012.

Wulfmeyer, V., R. M. Hardesty, D. D. Turner, A. Behrendt, M. P. Cadeddu, P. Di Girolamo, P. Schlüssel, J. Van Baelen, and F. Zus: A review of the remote sensing of lower tropospheric thermodynamic profiles and its indispensable role for the understanding and the simulation of water and energy cycles, Rev. Geophys., 53, 819–895, doi:10.1002/2014RG000476, 2015.

Yoshida, S., T. Sakai, T. Nagai, S. Yokota, H. Seko, Y. Shoji: Feasibility study of data assimilation using a mobile water vapor Raman lidar, Proceedings of the 19th conference on coherent laser radar technology and applications, 251-255, https://clrccires.colorado.edu/data/paper/P21.pdf, 2018a.

Yoshida, S., T. Sakai, T. Nagai, S. Yokota, H. Seko, and Y. Shoji: Data assimilation of water vapor mixing ratio observed by a lidar to forecast heavy precipitation, J. Meteor. Soc. Japan, (to be submitted), 2018b.